Research Article

Kouji Yasuda* and Toshiyuki Nohira

Electrochemical production of silicon

https://doi.org/10.1515/htmp-2022-0033
received September 30, 2021; accepted March 22, 2022

Abstract: Silicon solar cells are crucial devices for generating renewable energy to promote the energy and environmental fields. Presently, high-purity silicon, which is employed in solar cells, is manufactured commercially via the Siemens process. This process is based on hydrogen reduction and/or the thermal decomposition of trichlorosilane gas. The electrochemical process of producing silicon has attracted enormous attention as an alternative to the existing Siemens process. Thus, this article reviews different scientific investigations of the electrochemical production of silicon by classifying them based on the employed principles (electrorefining, electrowinning, and solid-state reduction) and electrolytes (molten oxides, fluorides, chlorides, fluorides–chlorides, ionic liquids [ILs], and organic solvents). The features of the electrolytic production of silicon in each electrolyte, as well as the prospects, are discussed.

Keywords: electrodeposition, electrorefining, molten salt, ionic liquid, organic solvent

1 Introduction

Silicon (Si) exists naturally as oxides or silicates, which are widely distributed in the earth's crust. In 1808, Berzelius produced ferrosilicon via the reaction of silica (SiO_2), carbon, and iron [1]. In 1811, Gray, Lussac, and Thenard produced impure amorphous Si by reacting silicon tetrafluoride (SiF_4) with potassium (K) metal [1]. In 1824, Berzelius first isolated Si by washing the reduction product of potassium hexafluorosilicate (K_2SiF_6) and K metal to remove the potassium fluoride (KF) byproduct and residual potassium metal from the silicide [1]. Further, Deville first prepared crystalline Si via electrodeposition in 1854 [2,3].

Silicon has been a very essential industrial material (ranging from structural to electronic ones) since the last half-century. Si exhibits many applications depending on its purity. Low-purity Si with 2 N (99%) purity, which is also known as metallurgical-grade Si (MG-Si), is utilized to produce alloys, such as silumin (Al–4~22%Si) and ferrosilicon (Fe–15~90%Si). MG-Si is also employed as an intermediate material for producing silicone resin and high-purity Si. High-purity Si is employed in semiconductor applications, such as large-scale integration (LSI) and solar cells. The required purities for LSIs and solar cells are 11–12 N (semiconductor-grade Si, SEG-Si) and 6–7 N (solar-grade Si, SOG-Si), respectively.

MG-Si is manufactured via the carbothermal reduction of silica stone or sand. Silica is reduced to MG-Si in arc furnaces equipped with carbon rod electrodes and operating at >2,000 K [4,5].

$$SiO_2(l) + 2C(s) \rightarrow Si(l) + 2CO(g). \quad (1)$$

The inhomogeneous temperature and material distributions induce complicated and multiple reactions. Various side reactions, such as the formations of silicon carbide (SiC) and silicon monoxide (SiO), occur and introduce impurities in the Si product and lower the reaction yield, respectively.

$$SiO_2(l) + 3C(s) \rightarrow SiC(s) + 2CO(g), \quad (2)$$

$$SiO_2(l) + C(s) \rightarrow SiO(g) + CO(g). \quad (3)$$

The final reaction, which yields Si, is regarded as the reduction of silicon oxides by a SiC reductant [6–9]:

$$SiO(g) + SiC(s) \rightarrow 2Si(l) + CO(g), \quad (4)$$

$$SiO_2(l) + 2SiC(s) \rightarrow 3Si(l) + 2CO(g). \quad (5)$$

Since the impurities in the raw SiO_2 and carbon reductant are included in the Si product, the purity and resistivity of MG-Si are 98–99% and 0.03 Ω·cm, respectively. The purity of the Si product did not exceed the 4 N (99.99%) level even when high-purity SiO_2 and high-purity carbon were utilized in the literature [10–14].

Historically, DuPont (in the 1960s) first industrialized the production of high-purity Si via the reduction of

* Corresponding author: Kouji Yasuda, Department of Materials Science and Engineering, Graduate School of Engineering, Kyoto University, Yoshida-honmachi, Sakyo-ku, Kyoto 606-8501, Japan, e-mail: yasuda.kouji.3v@kyoto-u.ac.jp, tel: +81-75-753-5430, fax: +81-75-753-5284
Toshiyuki Nohira: Advanced Energy Utilization Division, Institute of Advanced Energy, Kyoto University, Gokasho, Uji 611-0011, Japan

Open Access. © 2022 Kouji Yasuda and Toshiyuki Nohira, published by De Gruyter. This work is licensed under the Creative Commons Attribution 4.0 International License.

silicon tetrachloride ($SiCl_4$) with zinc (Zn) [15–18]. At the time, the DuPont process was challenging because of the removal of the residual Zn, as well as the avoidance of boron inclusion. Thereafter, DuPont's industrial method for producing high-purity Si was replaced by the Siemens process, which is based on hydrogen (H_2) reduction and/or the thermal decomposition of trichlorosilane ($SiHCl_3$) [19–22]. In the Siemens process, $SiHCl_3$, which is synthesized via the hydrochlorination of MG-Si, is purified and subsequently introduced into metallic bell jars. Further, H_2 reduction and/or thermal decomposition proceed on the Si rods, which are utilized as the heating elements and seed crystals that are installed inside the bell jars, at approximately 1,400 K. Single crystal ingots are manufactured from the produced polycrystalline Si via the Czochralski (CZ) method [23]. The floating zone method has also been employed to crystallize and further remove the impurities [24,25], although it has not been employed recently owing to the limited diameter of the produced crystal ingot.

The demand and production capacity of polycrystalline high-purity Si are shown in Figure 1(a) [26,27]. The demand was calculated by the authors of this review based on the reported production volume and specific Si weight of solar cells, e.g., 8 and 3.2 ton·MW^{-1} in 2000 and 2020, respectively. The proportion of SOG-Si in high-purity Si is shown in Figure 1(a). Before the year 2000, the ratio was <10% since the main product was SEG-Si, and the off-grade SEG-Si was supplied to the photovoltaic (PV) industry. The situation has changed drastically in the 21st century. The installation of PV cells has increased greatly (Figure 1(b)) in many countries owing to the necessity of renewable energy and financial supports [26,27]. The total capacity of installed PV cells was 138.2 GW in 2020, and it is increasing at the rate of 19%/year. In 2020, >90% of high-purity Si was utilized in the PV industry. Most Siemens processes were performed to yield SOG-Si as the main product. The production volumes were ~2.8 million tons and 480 thousand tons for MG-Si and high-purity Si, respectively, in 2019. All the high-purity Si were produced via the Siemens process.

Since some of the drawbacks of the Siemens process are its low productivity and high energy consumption, which are based on the gas-phase reaction, different SOG-Si production/Si purification methods have been developed and improved by researchers, particularly in the mid-2000s during which the short supply of SOG-Si was the bottleneck in the field. These processes can be divided into the three following categories: (a) the H_2 reduction and/or the decomposition of silane gases via the improved Siemen-based processes, (b) the metallothermic reduction of silicon halides by metal reductants, such as Zn and aluminum (Al), and (c) the purification of MG-Si via metallurgical purification methods. Each production process has been examined, and the details are published in review articles [28–63]. Historically, crystalline Si was first prepared (in 1854) by Deville via electrodeposition. Ever since, many methods for electrochemically producing Si have been investigated as alternative routes for producing high-purity Si. The details of each report were examined following the original literature and published review articles [64–70].

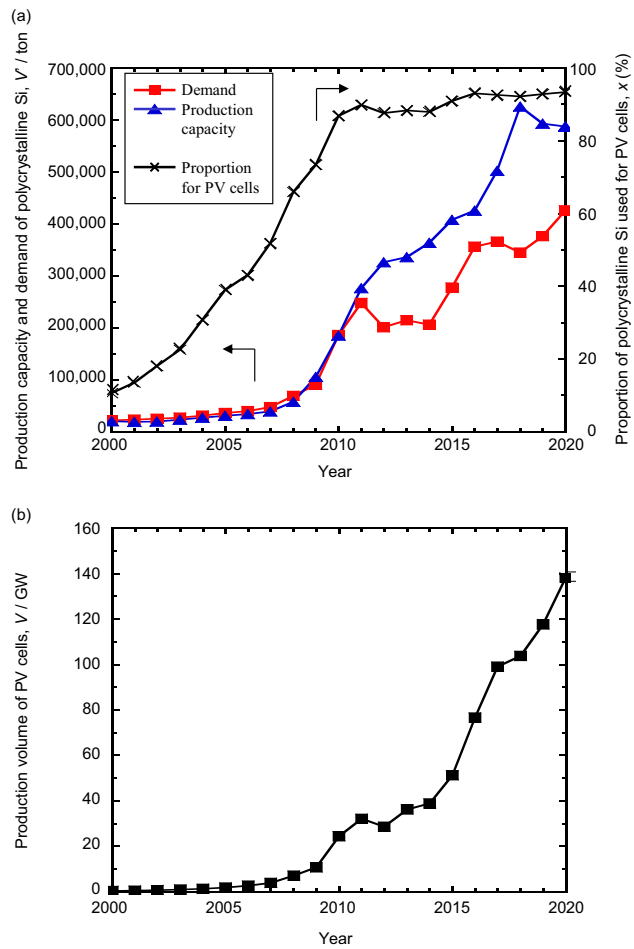

Figure 1: (a) Transition in production volume polycrystalline Si in the world and proportion of polycrystalline Si used for PV cells [26,27]. (b) Transition in production volume of PV cells.

Figure 2 shows the flowchart for the present and alternative production processes of substrate of Si solar cells. The processes are categorized as follows: (1) the refining of MG-Si to produce high-purity Si, (2) the production of bulk polycrystalline Si via high-purity Si compounds or high-purity silica using silica or MG-Si as starting materials, and (3) the direct formation of Si films on the substrate materials of solar cells via high-purity Si

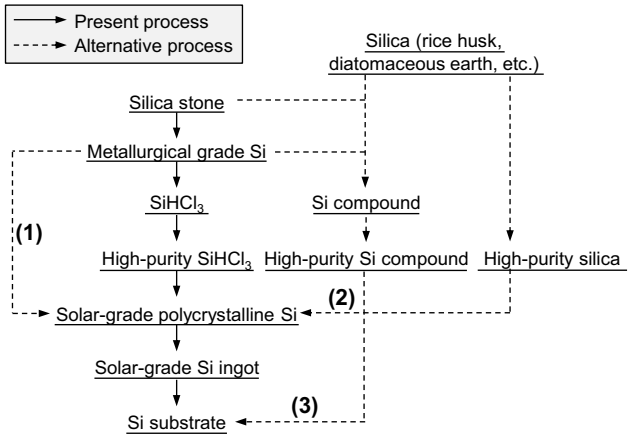

Figure 2: Flowchart for the present and alternative production processes of Si substrate for solar cells.

compounds or high-purity silica using silica or MG-Si as starting materials. A number of electrochemical processes have been reported for all these categories.

This study reviews the electrochemical processes for producing Si; these processes have been proposed or investigated based on classification, following the reaction principles: electrorefining, electrowinning, and direct solid-state reduction. Since many patents have been issued, the classification is mainly based on scientific papers. Further, the processes are also classified based on the utilized electrolyte (molten oxide, molten fluoride, molten chloride, molten fluoride–chloride, ionic liquid (IL), and organic solvent) in the reaction. The electrolytes are introduced in descending order of their operating temperatures. Regarding the mixed electrolytes, the reports are classified based on the species with the largest proportion; the components, except the Si species, are treated as the electrolytes. The foresight of this field is discussed based on the features of electrodeposition in each electrolyte.

2 Electrorefining

Regarding the electrorefining of Si, MG-Si was utilized as the feedstock for the anode. MG-Si was classified based on its contents of major impurities (Fe, Al, and Ca). The contents for standard grade 553 are lower than 0.5, 0.5, and 0.3 wt% for Fe, Al, and Ca, respectively. Other grades, such as 441, 3,303, and 2,202, are also commercially employed. The typical contents of the other impurities are 100–400 ppm each for Cr, Mg, Mn, Ni, Ti, and V and 20–40 ppm each for B, Cu, P, and Zn [42].

The behaviors of the impurities depend on the following ionization tendency: noble impurities precipitate as anode slime, while less-noble impurities dissolve and remain in the electrolyte. Contrarily, volatile impurities are removed as the vapor phase. One of the challenges of electrorefining is the enrichment of impurities in the electrolysis bath. Since impurity control in a continuous operation presents an inherent shortcoming, periodic bath cleaning, such as pre-electrolysis, is required. Regarding the continuous operation, the utilization of a liquid alloy comprising alloying elements, such as Cu, can be applied similarly to the electrorefining of Al metal known as the Hoopes process [71,72].

Massachusetts Institute of Technology (MIT) and Elkem proposed the electrorefining of Si in molten oxides employing liquid alloy cathodes, such as Cu–Si [73]. They proposed that the utilization of oxide electrolytes, $CaO–SiO_2$, $CaO–MgO–SiO_2$, $CaO–Al_2O_3–SiO_2$, and $BaO–SiO_2$, exhibiting melting points of <1,273 K would be beneficial.

Monnier and Giacometti reported the electrorefining in Na_3AlF_6 fluoride molten salts at 1,173–1,273 K [74–76]. They employed a dual-refining cell using a liquid Cu–Si alloy at the bottom. The current efficiency of the anode was ~100%, whereas it was 52.5–85% for the cathode. Olson and Carleton lowered the operation temperature to 1,023 K by employing an LiF–KF molten salt [77], after which they achieved the recovery of dense, coherent, and thick Si films on graphite and the vitreous carbon substrates. Sharma and Mukherjee performed continuous electrorefining in molten LiF–KF and recovered 67.4 g of the Si deposits [78]. The three-layer electrolysis of a Cu–Si anode/molten salt/Al cathode was reported by a group from Central South University [79]. Following a series of experiments, the selected optimum conditions were 1,023 K and 15 mol% K_2SiF_6 at 135 $mA·cm^{-2}$. A Norwegian group investigated electrorefining in $CaF_2–BaF_2$ [80,81] via experiments on a kilogram scale for 22 h. The obtained cathodic current efficiency was 97.2%. The changes in the morphology of the Si deposit under the electrolytic conditions have been reported by a Korean group [82].

Electrorefining in $CaCl_2$-based chloride melts has been reported by different groups, including Norwegian University of Science and Technology (NTNU) [83,84]. The utilization of an Si electrode as the anode in chloride molten salts induces passivation owing to the oxidation on the surface. Then, liquid alloys such as Si–Cu are necessary. The cathode deposit exhibited a powdery morphology, which was characteristic of the electrodeposition of Si in chlorides. Metallic Si anodes can be utilized in fluoride–chloride melts [85].

The refining ability depends on the difference between the standard redox potentials of the impurity and Si. Although the redox potentials vary with the electrolyte, B and Ti are generally difficult to remove [86].

Table 1: Electrorefining of Si proposed or investigated in the past

Author/affiliation, year, ref.	Electrolyte	Additive	Conc.	Temp. (K)	Cathode	Anode	Potential (cp), voltage (cv), current (cc)[a]	Morphology	Note
Molten oxide									
MIT and Elkem, 2007 [73]	$CaO–SiO_2$	SiO_2	40–75 wt%	1,923	C	Cu–Si	4.5 V (cv)	Lump	Other oxides can be applied as electrolytes
Molten fluoride									
Univ. Geneva, 1964 [74–76]	Na_3AlF_6	SiO_2	2–4 wt%	1,173–1,273	C and Si	Si and Cu–Si	200–1,000 $mA·cm^{-2}$ (cathode, cc)	Deposit	Cu–Si alloy was also used as an anode. Cathodic current efficiency was 52.5–85%
Solar Energy Res. Inst., 1981 [77]	LiF–KF	K_2SiF_6	Not given	1,023	C	Cu–Si	20–100 $mA·cm^{-2}$ (cathode, cc)	Dense, coherent, and thick film	n-type Si with 0.3–0.7 Ω·cm was produced
Bhabha Atomic Research Centre, 1986 [78]	LiF–KF	K_2SiF_6	6–18 mol%	923–1,023	C	MG-Si	77.5–232.5 $mA·cm^{-2}$ (cathode, cc)	Deposit	99.99% purity, continuous operation
Central South University, 2010 [79]	K_3AlF_6–LiF	K_2SiF_6	Not given	1,223	Al	Cu–Si	200–400 $mA·cm^{-2}$ (anode, cc)	Non-uniform powder	Three-layer electrolysis
Olsen et al., 2010 [80,81]	$CaF_2–BaF_2$	Not used	—	1,773	Si	Cu–Si	200–500 $mA·cm^{-2}$ (cathode, cc)	Ingot	The chronological change of impurities is investigated. B content was lowered by the addition of Ti and Fe
Ryu et al., 2012 [82]	LiF–KF	K_2SiF_6	1–9 wt%	973	Ag	MG-Si	23.8–71.7 $mA·cm^{-2}$ (cathode, cc)	Nodule, fiber, and whisker	Change in morphology for Si deposits
Molten chloride									
NTNU, 2012 [83,84]	$CaCl_2$–NaCl–CaO	Si and SiO_2	5 wt%	973–1,223	W and Si	Cu–Si	−0.75 V vs W (cp), −0.4 V vs Mo (cp)	Powder	The use of MG-Si anode was failed due to the passivation. Added Si was dissolved as metallic state
Molten fluoride–chloride									
Zou et al., 2012 [85]	KCl–NaF	—	—	1,073	Ni	MG-Si	2.0 V (cv)	Whisker	MG-Si can be directly used as an anode. No addition of Si source in the electrolyte in advance

[a]cp: constant potential electrolysis, cv: constant voltage electrolysis, cc: constant current electrolysis.
—: Not reported.

3 Electrowinning and Electrodeposition

Regarding the electrowinning of Si, silicon compounds are supplied into the bath as raw materials. Different compounds have been reported as feedstocks in the literature. A typical example is K_2SiF_6 since fluorosilicic acid (H_2SiF_6) is a byproduct of the acid treatment for producing phosphate fertilizer. K_2SiF_6 is prepared via the reaction of H_2SiF_6 with KF or KOH.

$$H_2SiF_6 + 2KF \rightarrow K_2SiF_6 + 2HF, \quad (6)$$

$$H_2SiF_6 + 2KOH \rightarrow K_2SiF_6 + 2H_2O. \quad (7)$$

The purity of K_2SiF_6 is typically 98–99% when bulk chemicals are employed in the reactions.

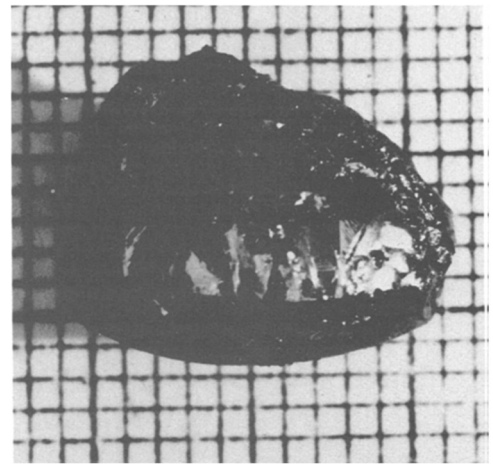

Figure 3: Photograph of electrodeposited Si weighing 1.6 g produced during an experiment from a $BaO–SiO_2–BaF_2$ melt (22.2:63.2:14.5 mol%) of 125 g for 50 h [87]. Permission from Electrochemical Society.

3.1 Molten oxide electrolytes

Elwell et al.'s group at Stanford University reported the electrowinning of liquid Si at different temperatures, such as 1,723 K, which were higher than its melting point [87–89]. They conducted the two-electrode electrolysis employing graphite electrodes in $BaO–SiO_2–BaF_2$ and $SrO–SiO_2–SrF_2$ electrolytes. The oxides and fluorides of the alkali and alkaline earth metals were added to facilitate the melting, thereby obtaining a Si lump (1.6 g with 99.97 wt%), as shown in Figure 3, with a current efficiency of 15–40%. The major impurities were Fe (200 ppm), Ca (30 ppm), Mn (20 ppm), Sr (10 ppm), and Ti (10 ppm) (Tables 1 and 2).

3.2 Molten fluoride electrolytes

There are abundant reports on the electrowinning and electrodeposition of Si in molten fluorides [89–119], and the representative studies are summarized in Table 3. The electrolysis conditions (electrolyte, Si additive, concentration, temperature, and cathode), methods (constant potential, constant voltage, and constant current), and obtained typical results (the existence of Si(II) ions, electrochemical reversibility, and morphology of the obtained Si) are also listed.

In the 1970s and 1980s, electrodeposition using fluoride molten salts was intensively studied at Stanford University. Cohen and Huggins reported the growths of Si substrates via constant electrolysis in LiF–KF and LiF–NaF–KF molten salts at <6 $mA·cm^{-2}$ [90–92]. At higher current densities, the morphology changed into grains with a size of 10–500 μm. Elwell et al. conducted a series of investigations as a project for the US Department of Energy (DOE) [93–99]. Therein, coherent Si films were formed on a graphite substrate at 10–60 $mA·cm^{-2}$; it was free from voids and exhibited a <111> texture in molten LiF–KF, following the addition of 8–14 mol% K_2SiF_6 at 1,118–1,123 K. The typical cross-sectional SEM images are shown in Figure 4 [94]. The deposited Si film exhibited n-type characteristics with a resistivity of up to 3 Ω·cm, the carrier mobility of 100 $cm^2·V^{-1}·s^{-1}$, and carrier concentration of 10^{17} atom per cm^{-3} [97]. The comproportionation reaction between the Si(IV) ions and deposited Si to form Si(II) ions was proposed because of the decreased current efficiency and smoother morphology with the growth of the film [94,95]. The homogeneous morphology of the Si electrodeposits was obtained by applying a current pulse (Figure 5(b)), whereas the dendrites were formed during the electrolysis at constant current (Figure 5(a)) [104]. The reports by Cohen and Huggins [90] and Moore et al. [108] confirmed that a smooth epitaxial Si film can be electrodeposited by employing crystalline Si as the cathode substrate (Figure 6).

The existences of Si(II) ions in these reports are inconsistent. Rao et al. first proposed the possibility of Si(II) formation in which they claimed that the dissolution of the deposited Si during the comproportionation of the Si(IV) ions to form the Si(II) ions would yield noncoherent deposits [93,95]. The formation of the Si(II) ion intermediates was reported via the half-peak potential in cyclic voltammetry (CV) [104], the current-reversal chronopotentiometry [105] in molten LiF–NaF–KF, and square-wave voltammetry (SWV) in molten LiF–KF and LiF–NaF–KF [112,113].

Table 2: Electrowinning and electrodeposition of Si in molten oxide electrolytes proposed or investigated in the past

Author/affiliation, year, ref.	Electrolyte	Additive	Conc. (mol%)	Temp. (K)	Cathode	Existence of Si(II)	Reversibility	Potential (cp), voltage (cv), current (cc)	Morphology	Note
Stanford Univ., 1981 [87–89]	$BaO–BaF_2–SiO_2$	SiO_2	63.2	1,666–1,738	Graphite	Suggested	–	0.8–16 V (cv)	Lump	15–40% current efficiency, 0.2 Ω·cm resistivity

Conversely, the existence of the Si(II) ions was denied via CV in LiF–KF [96] and NaF–KF [117], SWV in molten LiF–KF [116], as well as CV and open-circuit chronopotentiometry in $BaF_2–CaF_2$ [118]. The ionic affinity of the cations might account for the stability of the Si ions with lower valences.

Regarding the electrodeposition of the Si film from the SiO_2 feedstock in the fluoride melt, Elwell reported that the film was only recovered on a graphite substrate from molten $NaF–CaF_2$, and only traces of the Si deposit were recovered from the $MgF_2–NaF$, $KF–BaF_2$, $KF–CaF_2$, and $KF–MgF_2$ melts [100]. However, a dense Si film was deposited on a Mo substrate in a $BaF_2–CaF_2–SiO_2$ melt at 1,573 K [118]. The different results were attributed to the high temperature, as well as the formation of intermetallic compounds. Additionally, the changes in reduction potentials and Si morphologies were explained by Raman spectroscopy which analyzed the coordination states such as Si fluorides, oxyfluorides, and silicate ions [119,120]. The current efficiency for the deposition of Si from LiF–NaF–KF containing SiO_2 was limited to 10% at 873 K.

3.3 Molten chloride electrolytes

Table 4 lists the reports on the electrodeposition of Si in molten chlorides [121–128]. Although $SiCl_4$ gas was introduced into molten LiCl–KCl at 723 K, it barely dissolved in the melt [122]. The different stabilities of the Si species in the melt induced different volatilities between the fluoride and chloride melts. For example, Si(IV) ions are stable in fluoride melts as SiF_6^{2-}. However, such stable complex ions might not be formed in chloride melts. Further, the reaction to form Si(II) could lower the current efficiency for the electrodeposition of Si [124]. Recently, some groups from the University of Texas (Austin) and MIT have reported the photoelectrochemical properties for Si films that were electrodeposited in $CaCl_2$-based molten salts [125–127]. The introduction of O^{2-} ions facilitated the dissolution of SiO_2 in the melt, as well as the electrodeposition of the Si films, after which a compact and dense film (thickness = 35–40 μm) was obtained. The photoelectrochemical measurements in an organic electrolyte containing ethyl viologen cations (EV^{2+}) revealed the photoreduction current under illumination, thus demonstrating the p-type semiconductor for the electrodeposited Si (Figure 7). The impurity contents (Ti, Cu, Ni, Cr, and Fe) exerting harmful impact were below the tolerable threshold. However, the B and P contents were not measured here. When Al_2O_3 powder was added into the melt, a p-type Si film containing 10 ppm Al was obtained. Additionally, an

Table 3: Electrowinning and electrodeposition of Si in molten fluoride electrolytes proposed or investigated in the past

Author/ affiliation, year, ref.	Electrolyte	Additive	Conc.	Temp. (K)	Cathode	Existence of Si(II)	Reversibility	Potential (cp), voltage (cv), current (cc)	Morphology	Note
Cohen and Huggins, 1976 [90–92]	LiF–KF and LiF–NaF–KF	K_2SiF_6	1–10 mol%	873–1,123	Si (single crystal)	—	—	0.1–100 mA·cm^{-2} (cc)	Epitaxial and columnar grain	Epitaxial growth of Si was observed below 6 mA·cm^{-2}
Elwell et al., 1981 [93–99]	LiF–KF and LiF–NaF–KF	K_2SiF_6	0.5–16 mol%	1,018–1,023	Ag and Graphite	Suggested	Quasi-rev.	−0.40 to −0.86 V vs Pt (cp), 10–60 mA·cm^{-2} (cc)	Coherent film	Deposit with < 111 > texture and free from voids are produced
Elwell, 1981 [100]	NaF–CaF_2	SiO_2	13.8 mol%	1,423	Graphite	—	—	1.02 V (cv)	Particle	Si was not recovered from other fluoride melts
Boiko et al., 1982 [101,102]	NaF–KF	K_2SiF_6–SiO_2	39.5 mol%	983–1,053	—	—	—	300–3,000 mA·cm^{-2} (cc)	Powder and fiber	Current efficiency over 90%
Carleton et al., 1983 [103]	LiF–KF	K_2SiF_6	8 mol%	1,023	Vitreous carbon and graphite	Yes	—	40–70 mA·cm^{-2} (cc, step)	—	Initial nucleation behavior was investigated. Chronopotentiometry suggested the Si(II) ions
Bouteillon et al., 1983 [104,105]	LiF–KF and LiF–NaF–KF	K_2SiF_6 and Na_2SiF_6	0.05–5 mol%	1,023	Ag and graphite	Yes	Rev. (Irrev.)	5–40 mA·cm^{-2} (cc, pulse)	Dendrite and coherent film	The morphology changed from dendrite to coherent by current pulse technique
Stern and McCollum, 1985 [106]	LiF–NaF–KF	K_2SiF_6	10 wt%	1,023–1,043	Inconel	—	—	−0.7 to −1.3 V vs Pt (cp)	Smooth film	Instantaneous nucleation in initial stage
Moore et al., 1997 [108]	LiF–KF	K_2SiF_6	10 wt%	1,023–1,123	Ag and Si (single crystal and metallurgical)	—	—	10–150 mA·cm^{-2} (cc), 0.3 V (cv)	Epitaxial film and deposit	The use of silicon for cathode substrate leads to epitaxial growth
Sumitomo Chemical, 2007 [109–111]	Na_3AlF_6	SiO_2	5 wt%	973–1,573	Al	—	—	2.2 A (cc)	Lump (Si–Al alloy)	Mixed reaction between Al reduction and electrolytic reduction
NTNU, 2010 [112,113]	LiF–KF and LiF–NaF–KF	K_2SiF_6	5–20 mol%	823–1,073	Ag and Si (poly crystal)	Yes	—	21–41 mA·cm^{-2} (cc)	Dense coherent film	Si(II) ions were confirmed by square wave voltammetry and chronoamperometry

(*Continued*)

Table 3: *Continued*

Author/ affiliation, year, ref.	Electrolyte	Additive	Conc.	Temp. (K)	Cathode	Existence of Si(II)	Reversibility	Potential (cp), voltage (cv), current (cc)	Morphology	Note
Bieber et al., 2011 [116,117]	LiF–KF and NaF–KF	K_2SiF_6 and Na_2SiF_6	0.20–0.47 mol·kg^{-1}	973–1,223	Ag, graphite, and Ni	No	–	–	–	No existence of Si(II) ions was confirmed by square wave voltammetry
Hu et al., 2013 [118]	BaF_2–CaF_2	SiO_2	1.06×10^{-4} to 2.05×10^{-3} mol·cm^{-3}	1,573	Mo	No	Irrev.	118 mA·cm^{-2} (cc)	Dense film	Formation of intermetallic compound leads to production of dense film
Goto et al., 2015 [119,120]	LiF–NaF–KF	SiO_2	0.2–0.5 mol%	873	Ag	Unknown	–	0.2–1.4 V vs K^+/K (cp)	Smooth grain	Reduction potential varies by the coordination state

n-type Si film containing 3.5 ppm P was electrodeposited employing $Ca_3(PO_4)_2$ as an additive. When the p–n junction was formed by combining these Si films, a power conversion efficiency (PCE) of 3.1% was achieved with an open-circuit voltage of 295 mV and a short-circuit current density of 23.4 mA·cm^{-2} under a 100 mW·cm^{-2} illumination (Figure 8) [127]. This report represents a significant progress in the experimental demonstration of the electrochemical deposition of Si as a strategy for fabricating solar cells. The optimization of the electrolysis conditions is expected to increase the efficiency.

3.4 Molten fluoride–chloride electrolytes

The electrochemical production of Si in fluoride–chloride molten salts is summarized in Table 5. Fluoride–chloride melts have been studied since the 1960s in the Soviet Union [129–134]. Various types of fluoride–chloride melt such as KF–KCl, LiF–KCl–CsCl, and LiF–KCl, have been studied. Continuous and adherent Si layers were obtained on graphite and Si substrates in molten LiF–KCl–CsCl–K_2SiF_6 at 873–1,123 K [133,134]. Without pre-electrolysis, the morphology of the Si deposit became dendritic. The epitaxial growth proceeded on the Si substrate on which trihedral pyramids were observed. This study proceeded after the Soviet Union was renamed Russia [135–140]. The studies revealed that the deposition occurred as instant nucleation, following the diffusion-controlled growth. The addition of oxygen-containing species facilitated the change in the Si deposits from continuous planar into fiber and powder via the formations of the SiO_4^{4-} groups and oxyfluoride [137,141]. Another group at the Russian Academy of Science investigated the NaCl–KCl–NaF(10 wt%)–K_2SiF_6 system and observed that the reduction of the Si(IV) ions into metallic Si proceeded via a two-stage reaction [142]. The first and second reactions involved reversible and quasi-reversible electrochemical processes, respectively. Regarding the KF–KCl (+KI) systems, the electrodeposition of Si proceeded via the addition of K_2SiF_6 (+SiO_2) [135]. The grain size was reduced, following the addition of silica to the melt. Electrodeposition in KF–KCl molten salt was also reported by a group in Kyoto University; they focused on the high solubility of KF in water [143–146]. Although most fluorides exhibit low solubilities, KF exhibits exceptionally high solubility in water compared with the alkali and alkaline-earth fluorides (solubility to 100 g-H_2O at 298 K: KF, 101.6 g; LiF, 0.13 g; NaF, 0.15 g; MgF_2, 0.13 g; CaF_2, 0.0016 g). The reduction of Si(IV) ions into metallic Si was observed as a single 4-electron wave, which is explained by an E_qE_r (quasireversible-reversible electron transfer reactions) mechanism.

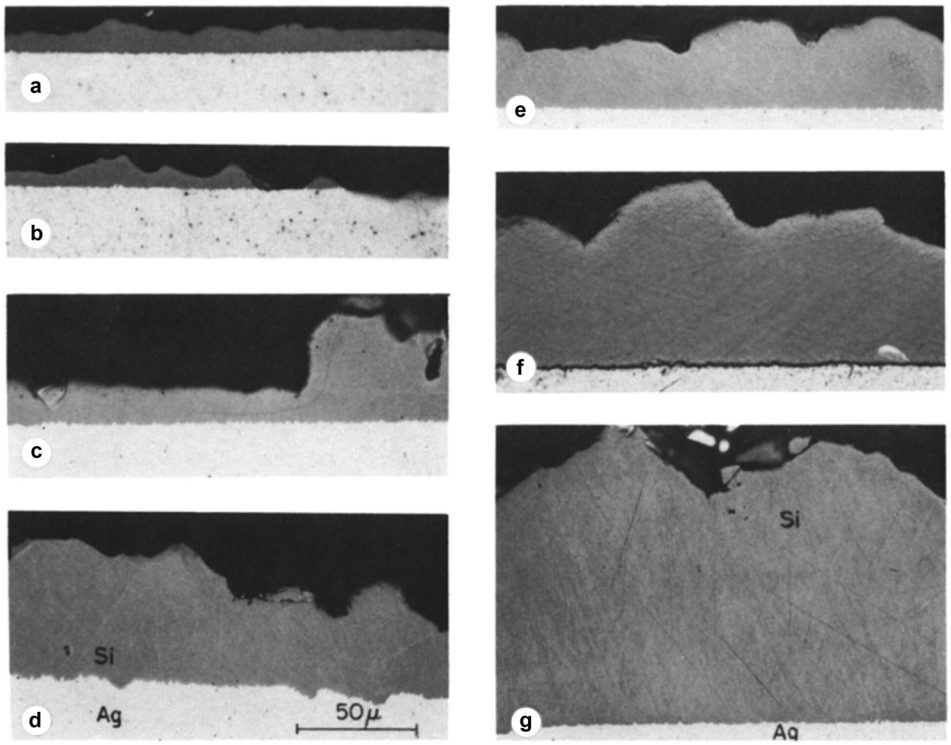

Figure 4: Cross-sectional SEM images of electrodeposited Si onto Ag substrates prepared at 25 mA·cm^{-2} in molten LiF–KF containing 12 mol% K_2SiF_6 at 1,023 K for (a) 1 h, (b) 1.5 h, (c) 2 h, (d) 3 h, (e) 4 h, (f) 6 h, and (g) 8 h [94]. Permission from Elsevier.

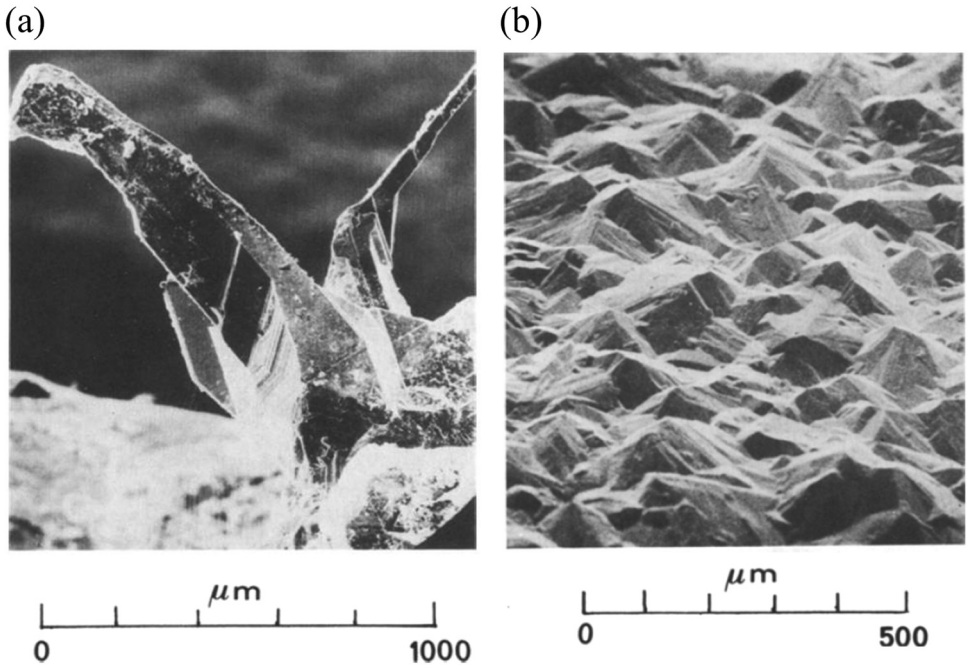

Figure 5: SEM images of electrodeposited Si prepared in molten LiF–NaF–KF containing 5 mol% Na_2SiF_6 at 1,023 K. (a) Constant current electrolysis at −20 mA·cm^{-2}. (b) Pulsed current electrolysis at −40 mA·cm^{-2} for 30 s, +40 mA·cm^{-2} for 1 s, and 0 mA·cm^{-2} for 60 s [104]. Permission from Springer.

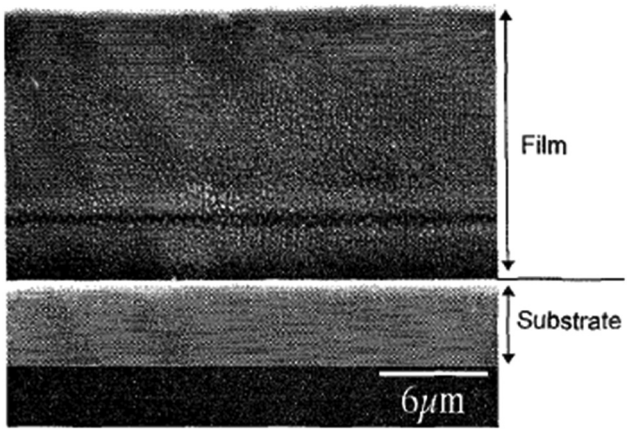

Figure 6: Cross-sectional SEM image of a stain-etched Si film deposited on single crystalline Si in molten LiF–KF containing 10 wt% K_2SiF_6 at 1,123 K [108]. Permission from IEEE.

The group proposed and experimentally demonstrated the utilization of $SiCl_4$ gas as a Si-ion source for electrodeposition, and continuous and smooth films were obtained in the KF–KCl–K_2SiF_6 melt [144–146]. A recent report by MIT and the University of Texas (Austin) revealed that the addition of a small amount of metallic tin (Sn) into the KF–KCl–K_2SiF_6 melt changed the morphology of the Si deposit from a nanowire to a dense film [147]. Further, the following photoelectrochemical measurements confirmed that the Sn-doped Si film was an n-type semiconductor. The recovery of the Si particles from the electrolyzed liquid Ga cathode in the KF–KCl–K_2SiF_6 molten salt was achieved by a group from NTNU and Kyoto University [148].

3.5 Ionic liquid electrolytes

Table 6 lists the reports for the electrodeposition of Si in IL electrolytes [149–167]. The abbreviations of the constituent species of ILs and their additives are defined in the footnote of the table.

Most studies employed bis(trifluoromethylsulfonyl) amide (TFSA)-based ILs and liquid $SiCl_4$ additives. The electrodeposited silicon in ionic liquids was readily oxidized during the treatment following the reduction; thus, its detection was difficult [149,153]. Furthermore, several reports have revealed that ILs were detected in the deposited Si layers. The deposition of Si is generally confirmed via X-ray photoelectron spectroscopy (XPS) at 99.5 eV for the Si 2p spectrum and Raman spectroscopy at 520 cm^{-1} for the transverse optical (TO) photons of crystalline Si or a smaller wavenumber due to the lack of long-range order for nanocrystalline/amorphous Si. In 2016, Zhang et al. observed the X-ray diffraction (XRD) peaks of crystalline Si at 28.4°, 47.3°, and 56.1° corresponding to the (111), (220), and (311) planes, respectively, for the deposit that was obtained by employing the liquid Ga cathode and [TBMA][TFSA] IL at 373 K [163]. The detection of crystalline Si via XRD was also reported by Shah et al. [164] and Zhao et al. [167]. The deposition process was analyzed by various techniques, including scanning tunneling microscopy (STM) [151,152] and electrochemical quartz crystal microbalance (EQCM) [157–159,165]. The smoothness of the Si film can be improved by light irradiation during electrodeposition [160]. Contrary to the electrodeposition in high-temperature molten salts, the voltammograms did not show any reduction current peak, and the diffusion coefficient of Si cations, as well as the existence of Si(II) ions, have not been reported. In addition to the Si film, Si nanowires with diameters and lengths of 10–100 nm and a few hundred microns, respectively, were obtained in [BMPy][TFSA] via repetitive two-potential electrolysis for the nucleation and growth stages [156]. They reported that the morphology of the wire accrued from the electrolysis pattern and not from the IL species. The effects of the anions on the deposition potential and characteristics of the Si deposits were negligible [161].

3.6 Organic electrolytes

The representative reports on the electrodeposition of Si in organic solvent electrolytes are listed in Table 7 [66,168–190]. The various abbreviations are also defined in the footnote of the table. Owing to the low ionic conductivities of organic solvents, supporting electrolytes whose information are included in the table are necessary. Many researchers have utilized propylene carbonate (PC), tetrahydrofuran (THF), and acetonitrile (AN) as organic solvents. Similar to the case of the ILs, the XRD verification of the deposition of crystalline Si was reported in the case involving the utilization of a liquid Ga electrode [187]. Other researchers have obtained amorphous Si films, except for ref. [179] that reported a small (111) peak for crystalline Si.

After a study in the mid-1960s [168], the deposition of Si in organic solvents was intensively investigated in Battelle [169–171] and the University of Southern California [172–174] as research projects for the DOE in the 1970s. Austin et al. obtained Si films in PC by adding $SiCl_4$ or $SiHCl_3$ and a supporting electrolyte. They obtained coarser deposits after adding the supporting electrolyte exhibiting

Table 4: Electrowinning and electrodeposition of Si in molten chloride electrolytes proposed or investigated in the past

Author/ affiliation, year, ref.	Electrolyte	Additive	Conc.	Temp. (K)	Cathode	Existence of Si(II)	Reversibility	Potential (cp), voltage (cv), current (cc)	Morphology	Note
Stern and McKenna, 1959 [121]	NaCl–KCl	K_2SiF_6	20 wt%	973–1,123	Fe	—	—	2.8–3.9 V (cv)	Deposit	The use of SiC anode
Matsuda et al., 1996 [122]	LiCl–KCl	$SiCl_4$	Not given	723	Si	—	—	–1.5 V vs Ag^+/Ag (cp)	Unknown	$SiCl_4$ hardly dissolved in chloride melt
Kongstein et al., 2007 [123]	$CaCl_2$–NaCl–CaO	Si	3.7 mol%	1,173	W and Mo	—	—	150 $mA{\cdot}cm^{-2}$ (cc)	Unknown	Fundamental research for electrorefining
Sakanaka et al., 2017 [124]	$BaCl_2$–$CaCl_2$–NaCl	SiO_2	1 mol%	923	Ag and Mo	Suggested	—	–1.2 to –1.7 V vs Ag^+/Ag (cp)	Porous sponge	Porous structure was suggested to be formed as a result of comproportionation reaction
Univ. Texas, Austin and MIT, 2017 [125–127]	$CaCl_2$–CaO	SiO_2 and $CaSiO_3$–SiO_2	3.9 mol%, 1.0–2.2 wt %	1,123	C	—	—	10–20 $mA{\cdot}cm^{-2}$ (cc)	Dense film	Photoelectrochemical measurement was carried out in EV^{2+} containing solution. PCE was 3.1% for the prepared p–n junction
Weng and Xiao, 2019 [128]	NaCl–$CaCl_2$	SiO_2	Saturated	1,073	C	—	—	0.3 V vs Ca^{2+}/Ca (cp)	Nanowire	Battery performance of Si nanowire for LIB was compared between electrodeposition and solid-state reduction

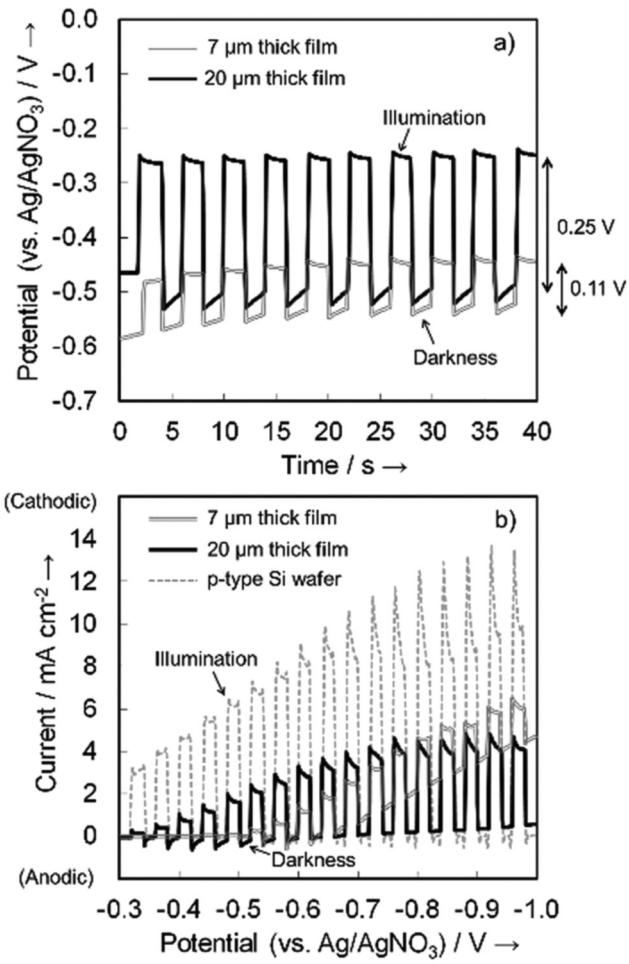

Figure 7: (a) Variation in open-circuit potentials and (b) photocurrent-potential characteristics for the deposited Si films and p-type Si wafer in darkness and under illumination at 100 mW·cm^{-2} [125]. Light interval was 2 s. Permission from Wiley.

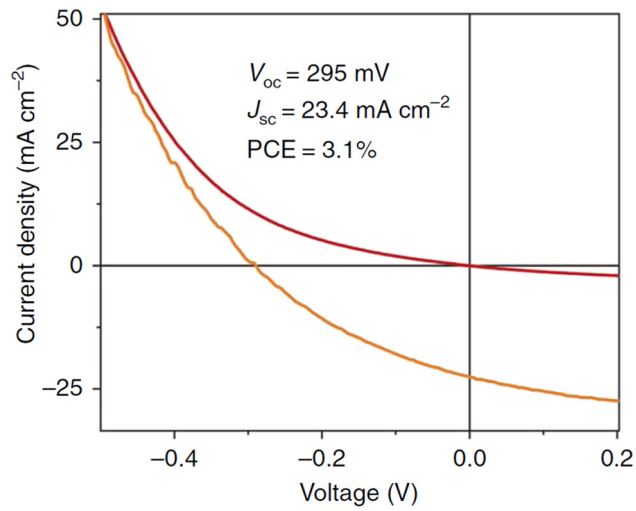

Figure 8: Current–voltage characteristics of the electrodeposited n-type silicon layer on p-type single crystalline silicon wafer under dark and under 100 mW·cm^{-2} illumination [127]. Permission from Springer Nature.

increased cation size (Figure 9). The boron doping of the Si film was achieved by adding $(C_4H_9)_4NBF_4$ into the electrolytic bath. The oxygen content was 3%, and the impurity level was <0.01%. Kröger et al. electrodeposited Si from an acetone solution containing HF and K_2SiF_6. Phosphorus doping, which was achieved by adding triethylphosphite to the electrolyte, reduced the resistivity, as well as changed the p-type character.

Since the reduction current for the electrodeposition appeared clearly, several papers reported the electrochemical analyses, such as the investigations of the formation of surface layers [180] and growth of Si deposits via chronoamperometry [182]. As well as the amorphous Si films produced via the physical vapor deposition (PVD) technique, the Si films electrodeposited in the organic solvents were highly hydrogen-terminated (Si:H). The chemical bonding of the amorphous Si deposits was analyzed via XPS and infrared (IR) spectroscopy. In addition to the Si–H bonding, the amorphous Si exhibited different bonds, such as Si–F and Si–C from EG–H_2SiF_6 [178] and Si–O and Si–C from THF–$SiCl_4$ depending on the compositions of the electrolyte [186]. The heat treatments induced the breaking of the Si–H bond, as well as the formation of Si–Si bond. The solar cell performance was also evaluated employing the electrodeposited Si. Nicholson constructed a heterojunction via the electrodeposition of a p-type Si layer on n-type Si wafers (Figure 10) [179]. The efficiency of this cell using Au and In–Ga alloy as electrical contacts was reported to be 1.8%. The same paper also reported the diode operation at junctions of the deposited Si layers and mercury contacts. Further, the photocurrent measurements were reported by a Polish group [189].

4 Solid-state reduction of SiO_2

The solid-state reduction of SiO_2 in molten chloride salts is another method for producing Si. Oki and Inoue first reported the solid-state electrochemical reduction of metal oxides in molten salts (TiO_2 in $CaCl_2$) [191]. Subsequently, Okabe et al. reported electron-mediated reaction as a method for reducing solid Nb_2O_5 into Nb metal via electrical connection to Ca metal in molten $CaCl_2$ [192]. The direct reduction of the metal oxides in molten chlorides was intensively studied after the report of the FFC-Cambridge process by Chen et al., in 2000 [193] on the

Table 5: Electrowinning and electrodeposition of Si in molten fluoride–chloride electrolytes proposed or investigated in the past

Author/ affiliation, year, ref.	Electrolyte	Additive	Conc.	Temp.	Cathode	Existence of Si(II)	Reversibility	Potential (cp), voltage (cv), current (cc)	Morphology	Note
Delimarskii et al., 1973 [130,131]	NaCl–KCl–NaF	Na_2SiF_6	0.5–3 wt%	973	C and Pt	Yes	—	—	—	The addition of NaF suppressed the decomposition of Na_2SiF_6 and evaporation of SiF_4
Boiko et al., 1975 [132]	KF–KCl	K_2SiF_6	0.27–2.5 × 10^{-4} mol·cm^{-3}	933	Ag and Pt	Yes	—	—	—	Mechanism was investigated by chronopotentiometry and linear sweep voltammetry
Russian Academy of Science, 1992 [133,134]	LiF–KCl–CsCl	K_2SiF_6	Not given	873–1,123	C, Si, Ge, W, Cu, Ni, and Fe	—	—	10–300 mA·cm^{-2} (cc)	Epitaxial, columnar, and dendritic	The effects of substrates, temperature, and pre-electrolysis on the Si morphology were studied
Kuznetsova et al., 2009 [142]	NaCl–KCl–NaF	K_2SiF_6	1.5–3.3 × 10^{-4} mol·cm^{-3}	1,023	Ag	Yes	Rev. (1st) Quasi-rev. (2nd)	−0.75 to −1.2 V vs C (cp)	Needle and flake	Diffusion coefficients were calculated
Russian Academy of Science, 2013 [135–140]	KF–KCl and KF–KCl–KI	K_2SiF_6 and SiO_2	0.5–13 mol%	923–1,073	Graphite, vitreous carbon, Ag, and W	No	Quasi-rev.	2–4 V (cv), 20–1,500 mA·cm^{-2} (cc)	Compact film, grain, nanowire, and fiber	SiO_2 addition leads to powder or fiber morphology. Deposition occurs as an instantaneous nucleation with diffusion-controlled growth
Maeda et al., 2015 [143–145]	KF–KCl	K_2SiF_6	0.5–5 mol%	923–1,073	Ag	—	Quasi-rev. (1st) Rev. (2nd)	10–500 mA·cm^{-2} (cc)	Compact film	The reduction of Si(IV) was explained by an E_qE_r mechanism. The optimum condition for compact and smooth film was investigated
Yasuda et al., 2017 [146]	KF–KCl	$SiCl_4$	2.3 mol%	923	Ag	—	—	155 mA·cm^{-2} (cc)	Compact film	Introduction of $SiCl_4$ gas to the melt supplies SiF_6^{2-} ions
MIT and Univ. Texas, Austin, 2018 [147]	KF–KCl	K_2SiF_6	1.0 mol%	923	C	—	—	5–20 mA·cm^{-2} (cc)	Dense film	The addition of tin to the electrolyte changed the Si morphology from nanowire to dense film
Haarberg et al., 2019 [148]	KF–KCl	K_2SiF_6	0.5 mol%	923	Ga	—	—	—	Particle	Si particles were recovered from liquid Ga cathode

Table 6: Electrowinning and electrodeposition of Si in ionic liquid electrolytes proposed or investigated in the past

Author/ affiliation, year, ref.	Electrolyte[a]	Additive[a]	Conc.	Temp.	Cathode	Potential (cp), voltage (cv), current (cc)	Morphology	Note
Katayama et al., 2001 [149]	[EMIm][TFSA]	$(EMIm)_2SiF_6$	1.08 M	298–363 K	Ag and Pt	−2.3 vs Ag (cp)	Film	The electrodeposited film contained Si. Deposition in pure Si additive was also studied
Endres et al., 2004 [150–152]	[BMPyrr][TFSA]	$SiCl_4$	Saturated, 0.1 M	296–298 K	C and Au	−1.6 to −2.7 V vs Fc^+/Fc (cp)	Film	Si film with 100 nm thickness was obtained and analyzed by STM
Nishimura et al., 2008 [153]	[TMHA][TFSA]	$SiCl_4$	0.1 M	293 K	Ni	−1.77 V vs Fc^+/Fc (cp)	Film	Deposition of Si film was confirmed by XPS and Raman spectroscopy
Nishimura et al., 2009 [154]	[EMPyrr]Cl–$ZnCl_2$	$SiCl_4$	Not given	423 K	Ni	0 V vs Zn^{2+}/Zn (cp)	Film	Thickness of 10 μm was obtained at 100 times faster rate than RT.
Martinez et al., 2010 [155]	[BMPyrr][TFSA]	$SiCl_4$ and $SiBr_4$	Saturated	298 K	Al and Ni	−2.2 to −2.5 V vs Ag and Pt (cp)	Film	The deposition occurred as three-dimensional with instantaneous nucleation
Fournier and Favier, 2011 [156]	[BMPy][TFSA]	$SiCl_4$	0.1–1 M	298 K	C	−1.0 to −2.6 V vs Pt (cp)	Nanowire	Diameter with 10–100 nm and length with a few hundred microns
Homma et al., 2013 [157–160]	[TMHA][TFSA]	$SiCl_4$	0.1–0.5 M	313 K	Au and Si	−2.0 to −3.0 V vs Pt (cp)	Film	The deposition of Si was analyzed by EQCM. Electrodeposition was performed during light irradiation
Endres et al., 2013 [161]	[BMPyrr][TfO], [BMPyrr][TFSA], and [BMPyrr][FAP]	$SiCl_4$	0.15 M	296–373 K	Au and Cu	−1.45 to −3.05 V vs Fc^+/Fc (cp)	Film	The behavior and deposits in three ionic liquids were compared
Park et al., 2013 [162]	[BMPyrr][TFSA]	$SiCl_4$	0.1–0.5 M	Not given	Au, Al, Cu, and Ag	−1.3 to −1.7 V vs Pt (cp)	Film	Observed XRD pattern was different from the standard powder pattern
Zhang et al., 2016 [163]	[TBMA][TFSA]	$SiCl_4$	0.25–0.5 M	373 K	Ga	−2.3 V vs Ag (cp)	Film and particle	Crystalline Si with XRD pattern was recovered by using liquid Ga as a substrate
Shar et al., 2017 [164]	[BMIm][TFSA]–[BMIm]PF_6	$SiCl_4$	0.1–1 M	298 K	C	−1.2 to −1.35 V vs Pt (cp)	Film	Small peak for crystalline Si was observed by XRD
Thomas et al., 2018 [165]	[BMPyrr][TFSA]	$SiCl_4$	0.04–1 M	298–373 K	Si	−2.7 to −3.2 V vs Pt (cp)	Film	The electrochemical reaction was studied by EQCM
Zhao et al., 2018 [166,167]	[BMIm][TFSA]–PC	$SiCl_4$	0.3 M–saturated	298–393 K	Ti, Ga, Ga–In, and Bi–In	−1.8 to −2.9 V vs Ag (cp)	Film	Mixture of IL and PC was also used as the electrolyte. Effect of liquid working electrode was investigated

[a]EMIm: 1-ethyl-3-methylimidazolium, BMPyrr: *N*-butyl-*N*-methylpyrrolidinium, TMHA: trimethyl-*n*-hexylammonium, EMPyrr: *N*-ethyl-*N*-methylpyrrolidinium, BMPy: 1-butyl-3-methylpyridinium, TBMA: tributyl(methyl)ammonium, BMIm: 1-butyl-3-methylimidazolium, TFSA: bis(trifluoromethylsulfonyl)amide, TfO: trifluoromethylsulfonate, FAP: tris(pentafluoroethyl)-trifluorophosphate.

Table 7: Electrowinning and electrodeposition of Si in organic electrolytes proposed or investigated in the past

Author/affiliation, year, ref.	Electrolyte[a]	Additive[b]	Supporting electrolyte[c]	Conc.	Temp.	Cathode	Potential (cp), voltage (cv), current (cc)	Morphology	Note
Austin et al., 1976 [169–171]	PC, THF, AN, DMS, TMS, and DMF	$SiCl_4$, SiF_4, and $SiHCl_3$	TEAC, TPAC, TPnAc, and THAC	0.02–1 M	308–418 K	Pt, Ti, Si, and Ti–Al–V	−2.5 to −2.6 V vs Pt (cp), 0.2–5 mA·cm^{-2} (cc)	Film	The addition of $(C_4H_9)_4NBF_4$ to the electrolyte enabled B doping to the film
Kröger et al., 1979 [172–174]	PC, CP, AC, acetone, EG, and FA	TEOS, silicic acid, and K_2SiF_6	TBAC and HF	0.0002– 0.1 M	298–358 K	Ni and SS	7–60 V (cv) 50 mA·cm^{-2} (cc)	Film	The bonding states of white, brown, or blue film was analyzed by IR
Takeda et al., 1981 [66,175]	AC and FA	TEOS and $(NH_4)_2SiF_6$	TMAC and TEAC	*ca.* 1.6–16 vol %, 0.14 M	298 K	Ni and Ti	0.4–15 mA·cm^{-2} (cc)	Film	Amorphous Si layer with 0.5 mm thickness was deposited
Gobet and Tannonberger, 1988 [176]	THF	$SiHCl_3$, $SiCl_4$, $SiBr_4$, TES, TEOS, SA, and TDMAS	$LiClO_4$, TBAB, and TBAP	0.1–1 M	Not given	Pt, Au, Ni, Cu, C, and ITO	−2.8 to −3.2 V vs Ag/AgCl (cp)	Film	No reduction in cyclic voltammetry for TES, TEOS, SA, and TDMAS additives
Sundersingh et al., 1992 [177,178]	EG	H_2SiF_6	—	0.02–0.5 M	298 K	SS and ITO	30–120 mA·cm^{-2} (cc)	Film	The use of supporting electrolyte is not needed
Nicholson, 2005 [179]	PC, THF, AN, DMS, and 1-MN	$SiCl_4$ and $SiBr_4$	TEAC, TPAC, TBAC, LiCl, TEAB, TPAB, TBAB, and LiBr	0.009–1.24 M	Not given	Si and Ti	0.3–1.25 mA·cm^{-2} (cc)	Film	The formation of an electrodeposited p-type Si/crystalline n-type Si heterojunction exhibited a solar cell efficiency of 1.8%
Munisamy and Bard, 2010 [182]	AN and THF	$SiCl_4$, $SiHCl_3$, $SiBr_4$, and SiI_4	TBAC	0.3 M	Not given	Pt, Ni, Ag, and C	−2.0 to −2.4 V vs Pt (cp)	Film	The initial stage of electrodeposition was analyzed by chronoamperometry
Philippe et al., 2012 [185,186]	AN, DCM, and THF	$SiCl_4$	TEAC and TBAC	0.3–1 M	298 K	Au	−1.0 to −5.0 V vs Pt (cp)	Film and porous film	The film became porous at negative potential due to gas evolution
Gu et al., 2013 [187]	PC	$SiCl_4$	TBAC	0.5 M	353–373 K	Ga	20 mA·cm^{-2} (cc)	Powder	Crystalline Si with XRD pattern was recovered by using liquid Ga as a substrate

[a]PC: propylene carbonate ($CH_3C_2H_3O_2CO$), THF: tetrahydrofuran ($(CH_2)_4O$), AN: acetonitrile (CH_3CN), DMS: dimethyl sulfate ($(CH_3O)_2SO$), TMS: tetramethylene sulfone ($(CH_2)_4SO_2$), DMF: dimethylformamide ($(CH_3)_2NCHO$), EG: ethylene glycol ($(CH_2OH)_2$), FA: formamide ($HCONH_2$), CP: 1-chloropropane (C_3H_7Cl), AC: acetic acid (CH_3COOH), 1-MN: 1-methyl naphthalene ($CH_3C_{10}H_7$), DCM: dichloromethane (CH_2Cl_2).

[b]TEOS: tetraethyl orthosilicate ($Si(OC_2H_5)_4$), TES: tetraethylsilane ($Si(C_2H_5)_4$), SA: silicon acetate ($Si(OOCCH_3)_4$), TDMAS: tetrakis(dimethylamino)silane ($Si[N(CH_3)_2]_4$).

[c]TEAC: tetraethylammonium chloride ($((C_2H_5)_4N)Cl$), TPAC: tetrapropylammonium chloride ($((C_3H_7)_4N)Cl$), TPnAC: tetrapentylammonium chloride ($((C_5H_{11})_4N)Cl$), THAC: tetrahexylammonium chloride ($((C_6H_{13})_4N)Cl$), TBAC: tetrabutylammonium chloride ($((C_4H_9)_4N)Cl$), TMAC: tetramethylammonium chloride ($((CH_3)_4N)Cl$), TBAB: tetrabutylammonium bromide ($((C_4H_9)_4N)Br$), TBAP: tetrabutylammonium perchlorate ($(C_4H_9)_4NClO_4$), TEAB: tetraethylammonium bromide ($((C_2H_5)_4N)Br$), TPAB: tetrapropylammonium bromide ($((C_3H_7)_4N)Br$).

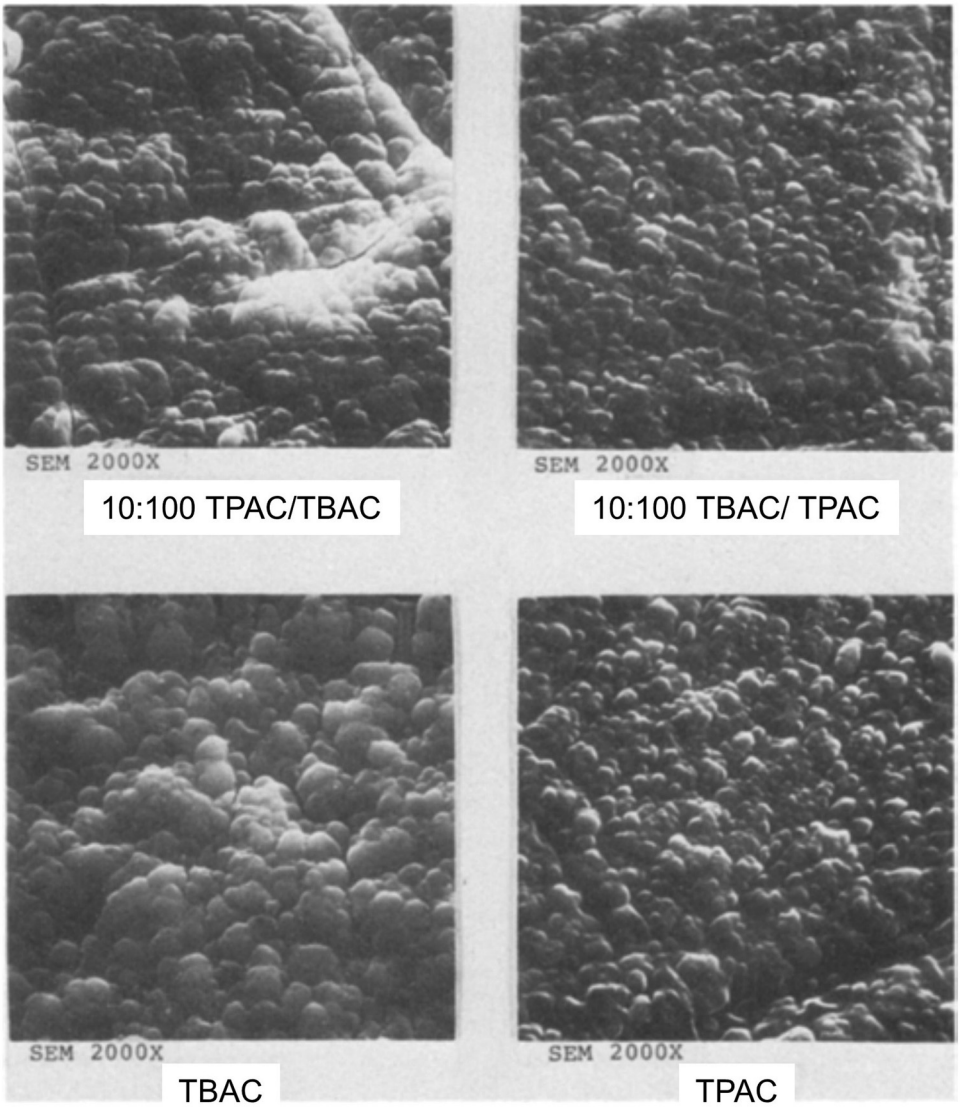

Figure 9: Surface SEM images of the Si films electrodeposited at 323 K in PC containing 1.0 M $SiHCl_3$ and various amount of TBAC and TPAC [171]. Permission from Electrochemical Society.

reduction of TiO_2 into Ti metal in molten $CaCl_2$ at 1,173 K. Additionally, the reductions of metal oxides into metals (metallothermic reduction) were also studied in molten salt [194–197]. The solid-state reductions of SiO_2 in molten chloride salts have been reported as a review paper [70] and as part of review papers on the direct reduction of metal oxides in molten salts [198–200].

Table 8 reveals that $CaCl_2$-based chloride salts were utilized as the electrolytes for the direct reduction of SiO_2 [201–236] owing to the high solubility of O^{2-} ions [237]. The basic information, such as the phase diagrams [237–239], properties of O^{2-} [240,241], and stable reference electrodes [205,242,243], which are necessary for the electrochemical studies of oxide reduction, were also reported. Moreover, the equilibrium potentials for the formation of Si–Ca alloys have also been reported [228]. Regarding the direct reduction of SiO_2, its contact with conducting materials, such as Mo [201], W [209], metallic Si [215], and carbon [227,229], is utilized as a current collector since solid SiO_2 is an electronic insulator even at high temperatures. Thus, it can be directly reduced into porous solid Si in molten $CaCl_2$ by a conducting material (Figure 11).

The reaction mechanism of the reduction of solid SiO_2 into Si is explained by the three-phase boundary model (conductor/insulator/electrolyte), which was established employing the point-contact electrode method [201,203] and SiO_2-sheathed electrode method [209,212] (Figure 12). The kinetics of the formation of the three-phase boundary is

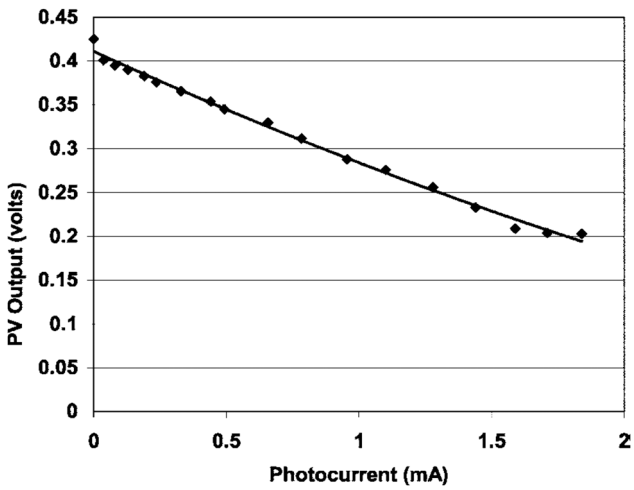

Figure 10: Photocurrent characteristics of an electrodeposited p-type Si layer onto n-type Si wafers [179]. Permission from Electrochemical Society.

well elucidated employing a thin-layer model that was proposed and experimentally confirmed during the solid-state reduction of AgCl in aqueous solutions [210,212,244]. The reduction proceeded at the contact point between SiO_2 and the conducting material. Thus, the contact point became a three-phase boundary between SiO_2, $CaCl_2$, and the conducting material. At the initial stage of the reduction, SiO_2 at the three-phase boundary was reduced by the electrons, which were directly supplied by the conducting material.

$$\begin{aligned} &SiO_2(s) + 4e^-(\text{through a conducting material}) \\ &\rightarrow Si(s) + 2O^{2-}\ (\text{in molten salt}). \end{aligned} \tag{8}$$

The byproduct, O^{2-} ions, was removed from the cathode via diffusion into the molten $CaCl_2$. Following the reduction of SiO_2 into Si, it exhibited high electrical conductivity at a high temperature to generate additional electron pathways. Further, the volume decreases from SiO_2 ($27.2\,cm^3{\cdot}mol^{-1}$) to Si ($12.1\,cm^3{\cdot}mol^{-1}$ for the crystalline Si) induced the formation of vacant spaces between the Si products, and these spaces were immediately filled with molten salt. These behaviors induced a new three-phase boundary inside the electrode (SiO_2, the penetrated molten $CaCl_2$, and the produced Si), after which the reduction occurred at the new three-phase boundary.

$$\begin{aligned} &SiO_2(s) + 4e^-\ (\text{through a produced Si}) \\ &\rightarrow Si(s) + 2O^{2-}\ (\text{in molten salt}). \end{aligned} \tag{9}$$

The reduction proceeded via the continuous production of new three-phase boundaries in the entire SiO_2 layer. The process is much faster on the SiO_2 surface than in the depth direction. The reduction rate was determined via the diffusion of the O^{2-} ions in the molten $CaCl_2$ filled in the produced porous Si layer [203,212]. The reported transfer coefficient, α, of the electroreduction of SiO_2 into Si was ~0.01 [210]. The unusually small value of α indicates its slow nuclear configuration and considerable resistance of the Si product. Further, considerable resistance was also proposed in the form of contact resistance for the reduction of the SiO_2 granules [212,228].

The mechanism of the direct reduction of SiO_2 is different from that of the FFC process for metal oxides, such as TiO_2, Nb_2O_5, NiO, and UO_2. The reduction of these oxides proceeds via the electrons that were supplied by the oxides.

$$\begin{aligned} &MO_x(s) + 2xe^-\ (\text{through } MO_x) \\ &\rightarrow M(s) + xO^{2-}\ (\text{in molten salt}). \end{aligned} \tag{10}$$

Thereafter, the reduction of the metal oxides during the FFC process proceeded at the two-phase interface between the metal oxide and molten salt. The system is similar to the case of electrodeposition because it is composed of electron transfer (electrode) and an ion conductor (electrolyte). Contrarily, since silicon oxides exhibit very high electrical resistivity even at high temperatures, electrons must be supplied from the current collector [201,203]. Therefore, the reduction of SiO_2 proceeded at the three-phase boundary between the silicon oxide, molten salt, and conducting material according to the reactions (8) and/or (9).

In terms of the reaction at the three-phase boundary, the necessity of the current collector is similar to the electrochemical reactions at the gas electrodes in fuel cells and the active materials in Li-ion batteries (LIBs). Thereafter, the direct reduction of SiO_2 would be naturally treated differently from the FFC process owing to the different reduction mechanisms.

Conversely, the possibility of liquid-to-solid reactions is also proposed for the production of Si from SiO_2 [218]. In the liquid-to-solid reaction, which is known as the dissolution-to-deposition reaction, SiO_2 is first dissolved in the molten salt with a high O^{2-} concentration [205,218,242], after which Si is electrodeposited from the produced silicate ions. The formation of calcium silicates is experimentally confirmed [219,245], and the reduction behaviors at different O^{2-} concentrations can be visually understood employing a potential-pO^{2-} diagram in which pO^{2-} is defined as $pO^{2-} = -\log a_{O}^{2-}$ (a_{O}^{2-} is the activity of O^{2-} ions in the molten salt) [205]. Considering that the trace of the morphology of the Si product from the original SiO_2 varied among the reports [201,218], the reaction to form Si would be a mixed one involving the solid–solid and liquid–solid reactions, and the ratios of

Table 8: Electrolytic production of Si by solid-state reduction of SiO_2 in molten chloride electrolytes proposed or investigated in the past

Author/affiliation, year, ref.	Electrolyte	Temp. (K)	Morphology of SiO_2	Cathode/ current collector	Potential (cp), voltage (cv), current (cc)	Note
Kyoto Univ., 2003 [201–208]	$CaCl_2$	1,123	Plate and tube	Mo	0.5–1.2 V vs Ca^{2+}/Ca (cp)	SiO_2 plate was reduced by a contacting electrode method with Mo wire. SOG-Si production process was proposed
Wuhan Univ., 2004 [209–211]	$CaCl_2$	1,173	Tube	W	−0.65 to −0.95 V vs Ag^+/Ag (cp)	W wire sheathed with SiO_2 was used as an electrode to evaluate the reaction kinetics by three-phase interline model
Wuhan Univ., 2004 [209,212,213]	$CaCl_2$	1,173	Powder	W	−0.6 to −1.1 V vs Ag^+/Ag (cp), −2.8 V vs graphite (cv)	SiO_2 powder inserted into a drilled hole for W plate was reduced to Si
Kyoto Univ., 2005 [214]	$LiCl–KCl–CaCl_2$	773	Plate	Mo	0.5–1.0 V vs Li^+, Ca^{2+}/Li-Ca (cp)	Amorphous Si was produced at 773 K
Kyoto Univ. 2005 [207,208,215–217]	$CaCl_2$	1,123	Pellet	Mo	1.0–1.2 V vs Ca^{2+}/Ca (cp), −2.6 to −2.8 V vs graphite (cv)	Reduction rate was accelerated by the use of (SiO_2 + Si) pellet. The use of Si rod avoids a contamination from a conducting material
Wuhan Univ., 2006 [212,213,218]	$CaCl_2$	1,173	Pellet	W	−0.6 to −1.1 V vs Ag^+/Ag (cp), −2.2 to −2.4 V vs graphite (cv)	Reaction was evaluated by three-phase interline model. Solubility of $CaSiO_3$ was measured to examine a dissolution-electrodeposition process
Univ. Pretoria, 2006 [219]	$CaCl_2$	1,173	Pellet	Ni	−2.0 to −2.5 V vs graphite (cv)	In addition to Si, $CaSiO_3$ was formed
Korea Atom. Ener. Res. Inst., 2008 [220]	$LiCl–Li_2O$	923	Dispersed powder	SS	−1.2 A (cc), electrode area was not given.	SiO_2 powder dispersed in a porous magnesia basket was reduced on SS rod
Ener. Mater. Tech. Inst., 2009 [221]	$CaCl_2$	1,173	Pellet	Mo	−1.2 V vs Pt (cp)	Si nanowire was formed by electrolytic reduction of SiO_2 pellet. Nanowires grew along the axial direction
Univ. Cambridge, 2010 [222,223]	$CaCl_2$	1,123	Compact layer on Si wafer	Mo and Si	−1.0 to −1.25 V vs graphite (cp)	Surface SiO_2 layer grown on Si wafer was reduced to porous Si with spherical morphology with submicron diameters
Middle East Tech. Univ., 2011 [224]	$CaCl_2$ and $CaCl_2–NaCl$	1,023–1,123	Pellet	SS, Ni, and Kanthal	−2.8 V vs graphite (cv)	Reduction rate was faster in $CaCl_2$ than $CaCl_2–NaCl$. The effect of temperature on reduction rate was small
Univ. Texas, Austin, 2012 [225–227]	$CaCl_2$	1,123	Dispersed powder	C, Ag, and Mo	0.4–0.45 V vs Ca^{2+}/Ca (cp), 2–8 $mA·cm^{-2}$ (cc)	Si was deposited in the $CaCl_2$ melt containing dispersed SiO_2 nano powders. Photoresponse of Si product was measured
Kyoto Univ., 2013 [228–231]	$CaCl_2$	1,123	Powder	Mo and C	0.5–0.7 V vs Ca^{2+}/Ca (cp)	Measured current density reached 0.7 $A·cm^{-2}$
Chinese Academy Sci., 2013 [233]	$CaCl_2$	1,123	Plate	Ni	−1.7 to −2.2 V vs graphite (cv)	Freestanding Si nanowire array was synthesized by using a dense plate and high contact density with a Ni net
Kyoto Univ., 2015 [234,235]	$CaCl_2$	1,123	Powder	Zn	0.9 V vs Ca^{2+}/Ca (cp)	SiO_2 was reduced to liquid Si–Zn alloy and then Si particles were precipitated during cooling

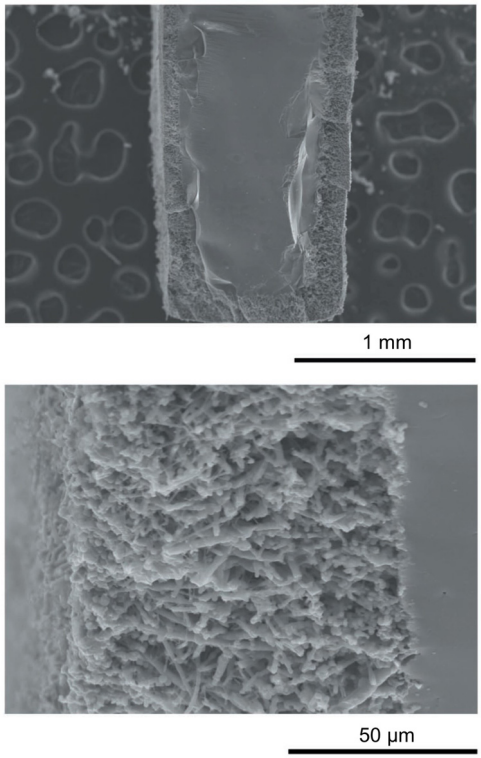

Figure 11: Cross-sectional SEM images of the reduction product obtained by potentiostatic electrolysis of a SiO_2 plate at 1.0 V vs Ca^{2+}/Ca in molten $CaCl_2$ at 1,123 K [201]. Permission from Springer Nature.

these reactions change with conditions, such as the salt composition and electrolysis potential. Further investigations based on quantitative analyses are necessary to control the morphology and purity of the Si product.

Studies are ongoing to determine the various applications, such as the production of SOG-Si, the fabrication of surface texture, and the formation of nanofibers, of electrodeposited Si. To produce SOG-Si, high-purity SiO_2 was reduced into high-purity Si during molten salt electrolysis. Thus far, the impurity level, except those of B and C, was lower than the acceptable level for application, and the current density (0.7 A·cm^{-2}), which was as large as the value for the commercial Hall-Héroult process for producing Al, was achieved at the initial stage of the reduction [230].

5 Discussion

5.1 Features of each electrolyte

The foregoing chapters introduced and categorized the electrochemical production of Si, as previously investigated.

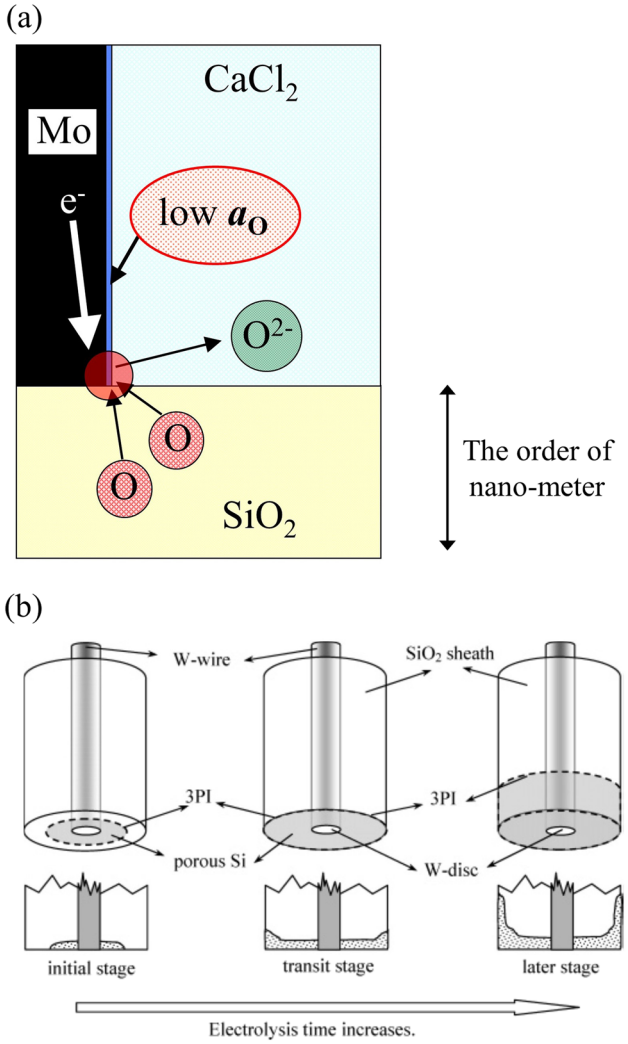

Figure 12: Schematic illustrations of the reaction mechanism proposed by using (a) a point-contact electrode method [203], and (b) a SiO_2-sheathed electrode method [210]. Permission from Springer Nature and American Chemical Society.

Table 9 summarizes the number of scientific papers regarding each electrolyte in each decade from the 1960s to the 2010s. Here the reports and patents were basically excluded from the counting. In the 1980s, many studies on the electrodeposition in fluoride molten salts were reported as research results of national projects, such as the Solar Array Project by the DOE in the USA. Further, many papers were published on electrodeposition in ILs, as well as the direct electrolytic reduction of SiO_2, following their discovery in the 2000s. This increase correlates with the recent high demand for solar cells and high-purity Si.

Si has been mainly studied electrochemically for its application in SOG-Si, while some studies have focused on anode materials for LIBs [183,184,190]. The features of each electrolyte are listed in Table 10. A high temperature

Table 9: Trend of scientific papers reported on electrochemical production of Si

Electrolyte type	Age						Sum
	1960s	1970s	1980s	1990s	2000s	2010s	
Molten oxide	0	0	2	0	0	0	2
Molten fluoride	1	1	17	1	0	14	34
Molten chloride	0	0	0	1	0	6	7
Molten fluoride–chloride	1	2	1	2	1	11	18
Ionic liquid	0	0	0	0	6	12	18
Organic solvent	1	0	6	2	3	8	20
Solid-state reduction of SiO_2	0	0	0	0	13	22	35
Sum	3	3	26	6	23	73	134

favors the production rate. However, the material selection of the electrolysis apparatus, as well as the volume shrinkage that are associated with the cooling procedure, is challenging. In the case that the generated Si is solid, the solubility of the constituent salts in water is also important because the adhered molten salts have to be washed. Furthermore, when the feedstock is SiO_2, one of the challenges is to develop oxygen evolution anodes. The challenges accompanying ILs and organic solvents include the low reaction rate and the low crystallinity of the Si deposits. The deposits are generally amorphous, and crystalline Si was obtained only under limited conditions. Since amorphous Si solar cells exhibit drawbacks, such as low conversion efficiency and light deterioration, their applications are presently limited. The highest hurdle of ILs is the anodic reaction rather than the deposition of Si. According to Zhang et al., the evolution of Cl_2 did not proceed at the anode even with the addition of Cl^- ions to $BMIMBF_4$ [246]. Regarding sustainable electrowinning, the additive must be decomposed as the total reaction between the anode and cathode. The development of ILs and anode materials, which facilitated Cl_2 evolution, greatly contributed to continuous electrowinning via the addition of $SiCl_4$.

5.2 Morphology control

The morphology of the Si products highly depends on the electrolytes. Typically, among the high-temperature molten salts, the deposition of a dense and flat morphology is possible with fluorides and fluoride–chlorides as listed in

Table 10: Feature of each electrolyte on electrochemical production of Si

Electrolyte type	Advantage	Disadvantage
Molten oxide	– Ultra-high reaction rate	– Selection of structural materials – Oxygen evolution anodes not yet developed – Volume shrinkage
Molten fluoride	– High reaction rate – Flat deposit	– Low solubility to water – Generation of fluorine compounds – Volume shrinkage
Molten chloride	– High reaction rate – High solubility to water – Cl_2 generation	– Low solubility of Si compound – Volume shrinkage
Molten fluoride–chloride	– High reaction rate – High solubility to water – Flat deposit	– Volume shrinkage
Ionic liquid	– Room temp. operation	– Low reaction rate – Unknown anodic reaction – Low crystallinity
Organic solvent	– Room temp. operation	– Low reaction rate – Low crystallinity
Solid-state reduction of SiO_2	– High reaction rate (initial)	– Porous product – Oxygen evolution anodes not yet developed – Decreased reaction rate of O^{2-} diffusion control (with the progress)

Tables 3 and 5, respectively. The oxides in the molten salts account for the key factor that determines the morphology. Zaykov et al. reported that the fluorides, oxyfluorides, and silicate silicon complexes were formed via the addition of oxides, which hindered the flat deposition of the Si layer [135,137]. The deposition of fibrous and granule Si in the oxide-containing melt has also been reported by other groups [100–102,119,124] except recent papers that reported the deposition of a dense and flat Si layer from $CaCl_2$–CaO–SiO_2 melts [125,126]. Moreover, other factors would determine the morphology of the deposits.

During low-temperature electrodeposition in ILs and organic solvents, the formation of a dense and flat Si film was generally achieved. This tendency might be closely related to the large overpotential that is required for the deposition at low temperatures since the morphology is typically dendritic when the reaction is governed by the diffusion of the ionic species.

In aqueous solution systems, the influence of the factors on the morphology of the deposit has been discussed employing the so-called Winand diagram [247–249], which affords the stability of Fischer's types of electrodeposits [250] as a function of two main parameters, namely the ratio of the current density to the diffusion-limiting current density and the inhibitions, such as the organic additives, exchange current densities, and hydrogen overvoltage. Even in high-temperature molten salts, the dependence of morphology on mass transfer, nucleation, and crystal growth provides insight into the electrocrystallization process. The relationship between the current density and ion concentration in molten KF–KCl was plotted and discussed employing the same methodology as that of the Winand diagram [144]. The optimum condition for electrodepositing a compact and smooth film was investigated as a function of the current density and the concentration of Si(IV) ions. The formation of the oxyfluoride complex ions (described above) would be an inhibition factor due to larger energy required for the desorption of ligands and larger distance between the Si atoms and the electrode surface than those for Si fluoride ions. The establishment of systematic theories in molten salts, as well as aqueous solutions, is desirable.

The direct electrolytic reduction of SiO_2 differs from the other cases in that the product becomes consistently porous owing to the volume decrease of SiO_2. Thus, the direct reduction of SiO_2 is not directly applicable to surface coating employing a compact Si layer. Instead, it exposes an effective pathway for synthesizing nanostructured Si, and several studies are ongoing to elucidate the phenomenon. The formation of Si nanowires via chemical vapor deposition requires the utilization of catalysts. However, such catalysts are not required in electrolytic methods; free-standing nanoarrays have been reported [221,233].

5.3 Purity control

In the discussion on the purity of Si and the PV performance, the level of the metal impurity is generally considered a determining factor. However, the C and O contents severely affected the PV performance. For instance, single-crystal pulling in the CZ method is impossible at C concentrations of $>5 \times 10^{18}$ atom per cm^3 since they become growth nuclei that interrupt the growth of the seed crystals [251]. Most previous studies utilized inductively coupled plasma-atomic emission spectroscopy (ICP-AES) on analyzing the impurity contents for the electrochemical production of Si. The measurements of the p–n characteristics and carrier concentrations by Elwell et al. [97] in the 1980s, as well as the photoelectrochemical measurements and formation of the p–n junctions by Bard et al. [125–127,226,227] in the 2010s, are desirable research works. Since the electrochemical production of Si is mostly aimed at PV applications, these evaluations must be driven by a collaboration with researchers in applied physics.

The target Si purity depends on the processes, i.e., the direct utilization of the Si films as solar cell substrates (Route (3), Figure 2) or the alternative of the Siemens process to produce high-purity polycrystalline Si (Route (2)). When the Si deposit is directly utilized (Route (3)), a high-purity of the 6 N level is required. By comparison, the required purity is less for producing polycrystalline Si (Route (2)). Thereafter, the polycrystalline Si product is cast into a mold to produce polycrystalline Si ingots; CZ pulling might also apply. High-purity Si is obtained from the feed polycrystalline Si in high yields because the metal impurities are enriched in the liquid phase during casting. However, the B, C, and P contents, which are challenging to remove via solidification refining owing to the high segregation coefficients, must be reduced at the stage of the feed polycrystalline Si.

In most studies, the Si precursors for the electrolysis utilize K_2SiF_6 in high-temperature molten salts and $SiCl_4$ in ILs and organic solvents. The drawback of utilizing K_2SiF_6 is the preparation of high-purity precursors. As described in Section 3, K_2SiF_6 is commercially manufactured via the neutralization of hexafluorosilicic acid with potassium hydroxide (Reactions (6) and (7)). Not only could metal impurities present limitations to the products,

but the inclusions of oxides and hydroxides can also be problematic. As discussed in Section 5.2, the addition of oxides into the molten salts would impact the morphology of the deposit into non-flat structures, such as granules and fibers. Conversely, rather than using SiO_2 itself as a precursor for electrolysis, it is appropriate to use it as a precursor for another compound. Rice husk [252–254] and diatomaceous earth [255–259] have also been proposed as the SiO_2 sources (shown as the arrows on the right side of Figure 2), and their reductions by C, Mg, electrons, etc., have been reported. For example, silica was first dissolved into an aqueous alkaline solution at pH 12.0 to remove heavy-metal impurities as precipitates [256,259]. Thereafter, the pH was controlled to 10.5 to yield high-purity silica. Solvent extraction employing 2-ethyl-1,3-hexanediol (EHD) with toluene as the solvent was employed to remove the light elements, including B [257–259]. Presently, high-purity SiO_2 is produced for optical applications via the reaction of $SiCl_4$ with O_2 or H_2O, which is produced by the chlorination of MG-Si. The high cost of production hinders its application in PV cells. High-temperature HCl leaching and the utilization of the Na_2SiF_6 byproduct of fertilizer have been proposed as potential sources of high-purity SiO_2 [10,11]. Electrowinning from the SiO_2 precursor is susceptible to carbon contamination because the anodic reaction corresponds to CO_2 evolution with a side reaction to produce CO_3^{2-} formation. In addition to carbon deposition from CO_3^{2-} anions, the impurities in the anode materials will be included in the melt to become potential impurities in the Si products. Regarding the electrochemical processes, it is necessary to establish a system that includes the anode materials and cell structure. From the standpoint of product quality, the impurities from the anode, particularly at high temperatures, represent the most challenging issue. For instance, in the molten $CaCl_2$ system that was investigated for the direct electrolytic reduction of SiO_2, the utilization of a carbon anode could make it difficult to avoid the deposition of C on the Si product at the cathode via the formation of CO_3^{2-} ions [219]. Although the solubility of CO_2 gas in the molten $CaCl_2$-based salt is not high [260], that of $CaCO_3$ is quite high [261] and the formation of CO_3^{2-} has been proposed [262–264]. In the case of inclusion of residual moisture in the electrolytes, the contamination issues also apply to the electrodeposition of Si layers other than the direct electrolytic reduction of SiO_2. Therefore, as mentioned in Section 5.1, the development of the contamination-free anodes is one of the most important tasks, including the oxygen evolution electrodes for the electrowinning from the SiO_2 feedstock.

The above discussion indicates that the utilization of $SiCl_4$ in high-temperature molten salts is promising. The preparation of inexpensive high-purity $SiCl_4$ can be accomplished via the carbochlorination of silica ores, followed by distillation. A research group at Kyoto University proposed the introduction of $SiCl_4$ as Si precursor for electrodeposition in fluoride–chloride mixed melt [143,146]. The supply of $SiCl_4$ gas into KF–KCl molten salt facilitated the following chemical reactions to form SiF_6^{2-} complex anions.

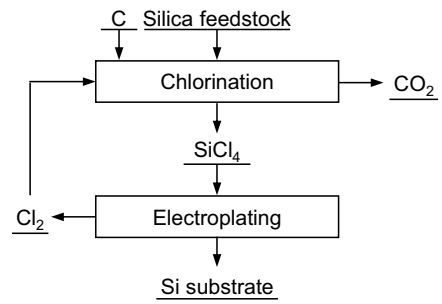

Figure 13: Flowchart for the electroplating in fluoride–chloride melt and the use of $SiCl_4$ precursor.

$$SiCl_4(g) + 6KF(l) \rightarrow K_2SiF_6(l) + 4KCl(l). \quad (11)$$

The feasibility of utilizing $SiCl_4$ as a precursor was verified through thermodynamic calculations, as well as electrochemical studies. A further advantage is that in the case of the fluoride–chloride mixed melt, the anodic reaction is the evolution of Cl_2 gas. In addition to preventing the impurity inclusion from the anode materials, the formed Cl_2 gas can be reused in the carbochlorination process, which ensured the establishment of a closed cycle (Figure 13). Although the solubility of $SiCl_4$ in the chloride melt is very low, it is highly soluble in fluoride–chloride melt via the ion-exchange reaction shown above. The high solubility allows for the fast electrodeposition of Si films.

To produce bulk polycrystalline SOG-Si, the utilization of liquid Si is theoretically promising for controlling the purity. Although a 6 N purity of Si is required for the PV applications, the purities that were achieved in past studies were at most 4 N level. Although a recent paper reported that the purity reached 99.99989%, the measured elements were limited and the exact purity was unknown [127]. The electrochemical fabrication of p–n junctions for solar cells makes great sense, but the process is very sensitive to product contamination, and significant hurdles remain in its realization in terms of required purity and quality stability. Another issue is that the technology for doping impurities into Si has not yet been established. Figure 14 compares the flowcharts for (a) direct production of solid Si and (b) production of Si utilizing liquid Si alloy as an intermediate product. In the direct production, most of the impurities from

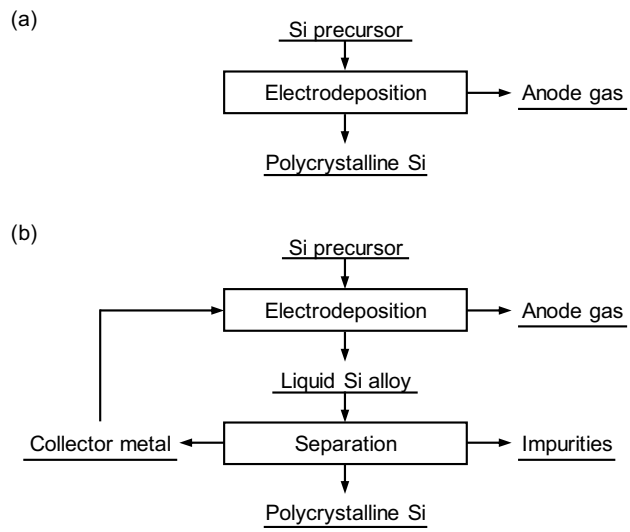

Figure 14: Flowcharts for the electrochemical production of Si in (a) direct production of solid Si and (b) production of Si by using liquid Si alloy as an intermediate product.

the Si precursor, anode material, molten salt, structural components of the electrolysis cell, etc., contaminate the Si products at the cathode. These impurities must be removed, if it is possible, by the washing treatment using, e.g., HCl aq. and HNO_3 aq. + HF aq. On the other hand, the process employing liquid Si alloy includes the purification step, following the electrolysis. During the separation of the solid Si phase from the liquid alloy, the impurities are concentrated in the remaining liquid phase according to the solid–liquid distribution, which ensures the production of high-purity Si. As well as the solidification refining at the solid Si–liquid Si [265], the segregation purification has been also investigated for various liquid alloys including Si–Al [266–282]. Since the continuous operation of the process (Figure 14(b)) enriches the impurities in the liquid phase, the purification, such as via distillation, of the collector metal is necessary after several runs. The establishment of a technology for efficiently precipitating solid Si from the liquid alloy is required.

6 Conclusion

In the past, SOG-Si was supplied from off-grade portions of SEG-Si that were manufactured via the Siemens process. Presently, many Siemens plants for producing SOG-Si production have been operating to deal with the increased demand for PV-based power generation. In the near future, as more and more electricity will be supplied by PVs, new types of SOG-Si production/Si purification processes will be required.

Electrochemical methods can potentially manufacture polycrystalline SOG-Si, and even facilitate the direct formation of solar cell substrates. The previously proposed or investigated electrochemical processes for producing Si were reviewed here by classification based on the reaction principles and employed electrolytes. Based on an overview of various reports, the important factors for Si electrodeposition such as morphology control and purity control were discussed. The aspects necessary for the establishment of future processes were also proposed.

The PV industry will definitely play a decisive role in the energy and environmental fields in the future. Therefore, the mass production of inexpensive SOG-Si is an urgent global task. Further research and development are required to establish the future production process.

Funding information: Authors state no funding involved.

Author contribution: KY and TN conceived the ideas for process evaluation. KY contributed the literature curation and writing the manuscript. KY and TN reviewed the manuscript.

Conflict of interest: Authors state no conflict of interest.

References

[1] Enhag, P. *Encyclopedia of the elements: Technical data – history – processing – applications*, Wiley-VCH, Weinheim, Germany, 2004.
[2] Deville, H. S. C. Comptes rendus hebdomadaires des séances de l'Académie des sciences. *Académie des Sciences*, Vol. 39, 1854, pp. 323–326.
[3] Weast, R. C., Ed. *CRC handbook of chemistry and physics*, 60th edition, CRC Press, Boca Raton, Florida, USA, 1980.
[4] Sirtl, E. *Proceedings of the 1st European Photovoltaic Solar Energy Conference, Luxemburg*, D. Reidel Publishing Company, Dordrecht, 1978, p. 84.
[5] Grabmaier, J., Ed. *Silicon/crystals: Growth, properties, and applications*, Springer-Verlag, Berlin, Heidelberg, New York, 1981, p. 57.
[6] Filsinger, D. H. and D. B. Bourrie. Silica to silicon: Key carbothermic reactions and kinetics. *Journal of the American Ceramic Society*, Vol. 73, No. 6, 1990, pp. 1726–1732.
[7] Müller, M. B., S. E. Olsen, and J. Kr Tuset. Heat and mass transfer in the ferro-silicon process. *Scandinavian Journal of Metallurgy*, Vol. 1, 1972, pp. 145–155.
[8] Schei, A. and O. Sandberg. Back reactions during production of silicon metal in a submerged arc electric furnace. *Selected topics in high temperature chemistry*. Forland et al., Universitetsforlaget, Oslo, Norway, 1966, pp. 141–150.
[9] Schei, A. On the chemistry of ferro-silicon production. *Tidsskr Kjemi, Bergves Metall*, Vol. 27, 1967, pp. 152–158.

[10] Aulich, H. A., K.-H. Eisenrith, H.-P. Urbach, F. W. Schulze, and J. G. Grabmaier. Preparation of high-purity starting materials for the production of solar-grade. *Silicon Siemens Forschungs und Entwicklungsberichte*, Vol. 11, No. 6, 1982, pp. 327–331.
[11] Aulich, H. A., K.-H. Eisenrith, and H.-P. Urbach. New methods to prepare high-purity silica. *Journal of Materials Science*, Vol. 19, No. 5, 1984, pp. 1710–1717.
[12] Aulich, H. A. and J. G. Grabmaier. Solar-grade silicon prepared by advanced carbothermic reduction of silica. *Siemens Forschungs und Entwicklungsberichte*, Vol. 15, No. 4, 1986, pp. 157–162.
[13] Amick, J. A., J. P. Dismukes, R. W. Francis, L. P. Hunt, P. S. Ravishankar, M. Schneider, et al. Improved high-purity arc-furnace silicon for solar cells. *Journal of the Electrochemical Society*, Vol. 132, No. 2, 1985, pp. 339–345.
[14] Sakaguchi, Y., M. Ishizaki, T. Kawahara, M. Fukai, M. Yoshiyagawa, and F. Aratani. Production of high purity silicon by carbothermic reduction of silica using AC-arc furnace with heated shaft. *ISIJ International*, Vol. 32, No. 5, 1992, pp. 643–649.
[15] Lyon, D. W., C. M. Olson, and E. D. Lewis. Preparation of hyper-pure silicon. *Journal of the Electrochemical Society*, Vol. 96, No. 6, 1949, pp. 359–363.
[16] Butler, K. H. and C. M. Olson. *Process for the production of pure silicon in a coarse crystalline form*. U.S. Patent, 2,773,745, 1956.
[17] Olson, C. M. *Preparation of Pure Silicon*. U.S. Patent, 2,804,377, 1957.
[18] Bertrand, L. *Production of Silicon*. U.S. Patent, 3,012,862, 1961.
[19] Schweickert, H., K. Reuschel, and H. Gutsche. *Production of high-purity semiconductor materials for electrical purposes*. U.S. Patent 3,011,877, 1961.
[20] Gutsche, H. *Method for producing highest-purity silicon for electric semiconductor devices*. U.S. Patent 3,042,494, 1962.
[21] Bischoff, F. *Method for producing pure silicon*. U.S. Patent 3,146,123, 1964.
[22] Reuschel, K. and A. Kersting. *Method of producing hyperpure silicon*. U.S. Patent 3,200,009, 1965.
[23] Czochralski, J. Ein neues Verfahren zur Messung der Kristallisationsgeschwindigkeit der Metalle. *Zeitschrift für Physikalische Chemie*, Vol. 92, 1918, id. 219 (in German).
[24] Pfann, W. G. Principles of zone-melting. *Transactions of the AIME*, Vol. 194, 1952, pp. 747–753.
[25] Keck, P. H. and M. J. E. Golay. Crystallization of silicon from a floating liquid zone. *Physical Review*, Vol. 89, No. 6, 1953, pp. 1297–1297.
[26] *Industrial rare metals, annual review 2021*, Vol. 137, Arumu Publishing Co, Tokyo, Japan, 2021.
[27] *Rare metal news*, Arumu Publishing Co, Tokyo, Japan, 2021.
[28] Uryu, T. Production methods of polycrystalline silicon. *Denki Kagaku*, Vol. 34, 1966, pp. 298–308.
[29] Spenke, E. and W. Heywang. Twenty five years of semiconductor-grade silicon. *Physica Status Solidi* (*A*), Vol. 64, No. 1, 1981, pp. 11–44.
[30] Dietl, J., D. Helmreich, and E. Sirtl. *"Solar" silicon. Silicon/crystals: Growth, properties, and applications*, Springer-Verlag, New York, 1981, pp. 43–107.
[31] Bathey, B. R. and M. C. Cretella. Solar-grade silicon. *Journal of Materials Science*, Vol. 17, No. 11, 1982, pp. 3077–3096.
[32] Lutwack, R. *A review of the silicon material task. DOE/JPL-1012-96*, 1984.
[33] Maeda, M. Production of high purity silicon and its market. *Seisan Kenkyu*, Vol. 38, No. 9, 1986, pp. 425–433.
[34] Kojima, T. and T. Furusawa. Application of fluidized bed reactors to production of polycrystalline silicon. *Kagaku Kogaku*, Vol. 51, No. 3, 1987, pp. 217–223.
[35] Moriyama, J. Production of high-purity silicon – an overview (I). *Suiyokwai-Shi*, Vol. 20, 1987, pp. 473–477.
[36] Moriyama, J. Production of high-purity silicon – an overview (II). *Suiyokwai-Shi*, Vol. 20, 1987, pp. 597–605.
[37] Moriyama, J. Production of high-purity silicon – an overview (III). *Suiyokwai-Shi*, Vol. 20, 1987, pp. 671–679.
[38] Moriyama, J. Production of high-purity silicon – an overview (IV). *Suiyokwai-Shi*, Vol. 21, 1989, pp. 52–58.
[39] Moriyama, J. Production of high-purity silicon – an overview (V). *Suiyokwai-Shi*, Vol. 21, 1989, pp. 195–200.
[40] O'Mara, W. C., R. B. Herring, and E. L. P. Hunt. *Handbook of semiconductor silicon technology*, Noyes Publications, Park Ridge, 1990.
[41] Kenkyukai, H. K. G., Ed. *Silicon no Kagaku* (*chemistry of silicon*), Realize Riko Center, Tokyo, 1992.
[42] Habashi, F., Ed. *Handbook of extractive metallurgy*, Vol. IV, Chap. 48, Wiley-VCH Publication, Weinheim, 1997, pp. 1861–1984.
[43] Kuramoto, M. Present and future of silicon materials processes. *Kinzoku*, Vol. 69, No. 11, 1999, pp. 935–942.
[44] Morita, K. Refining processes of silicon materials. *Kinzoku*, Vol. 69, No. 11, 1999, pp. 949–957.
[45] Woditsch, P. and W. Koch. Solar grade silicon feedstock supply for PV industry. *Solar Energy Materials and Solar Cells*, Vol. 72, No. 1–4, 2002, pp. 11–26.
[46] Gribov, B. G. and K. V. Zinov'ev. Preparation of high-purity silicon for solar cells. *Inorganic Materials*, Vol. 39, No. 7, 2003, pp. 653–662.
[47] Müller, A., M. Ghosh, R. Sonnenschein, and P. Woditsch. Silicon for photovoltaic applications. *Materials Science and Engineering: B*, Vol. 134, No. 2–3, 2006, pp. 257–262.
[48] Oda, H. Current status of silicon material for solar cells. *Kogyo Zairyo*, Vol. 55, No. 2, 2007, pp. 30–34.
[49] Takeshita, M., H. Ito, and Y. Hanaue. Polysilicon production in Mitsubishi Materials Corporation. *Journal of MMIJ*, Vol. 123, No. 12, 2007, pp. 704–706.
[50] Morita, K. and T. Yoshikawa. Problems and new solutions in the refining of solar grade silicon. *Materia Japan*, Vol. 46, No. 3, 2007, pp. 133–136.
[51] Tamamura, Y., et al., Eds. *Taiyo energy yuko riyo saizensen* (*frontier of effective use of solar energy*), NTS Inc, Tokyo, 2008 (in Japanese).
[52] Braga, A. F. B., S. P. Moreira, P. R. Zampieri, J. M. G. Bacchin, and P. R. Mei. New processes for the production of solar-grade polycrystalline silicon: A review. *Solar Energy Materials and Solar Cells*, Vol. 92, No. 4, 2008, pp. 418–424.
[53] Lynch, D. Winning the global race for solar silicon. *JOM*, Vol. 61, No. 11, 2009, pp. 41–48.
[54] Tang, K., E. J. Øvrelid, G. Tranell, and M. Tangstad. Critical assessment of the impurity diffusivities in solid and liquid silicon. *JOM*, Vol. 61, No. 11, 2009, pp. 49–55.

[55] Tang, K., E. J. Øvrelid, G. Tranell, and M. Tangstad. Thermochemical and kinetic databases for the solar cell silicon materials. *Crystal growth of si for solar cells*. Springer Berlin Heidelberg, Berlin, Heidelberg, 2009, pp. 219–251.
[56] Aratani, F. Current status of silicon raw materials for solar cells. *Journal of the Japanese Association of Crystal Growth*, Vol. 36, No. 4, 2010, pp. 246–252.
[57] Yasuda, K., K. Morita, and T. H. Okabe. Production processes of solar grade silicon by hydrogen reduction and/or thermal decomposition. *Journal of MMIJ*, Vol. 126, No. 4–5, 2010, pp. 115–123.
[58] Yasuda, K. and T. H. Okabe. Production processes of solar grade silicon based on metallothermic reduction. *Journal of the Japan Institute of Metals and Materials*, Vol. 74, No. 1, 2010, pp. 1–9.
[59] Yasuda, K. and T. H. Okabe. Solar-grade silicon production by metallothermic reduction. *JOM*, Vol. 62, No. 12, 2010, pp. 94–101.
[60] Johnston, M. D., L. T. Khajavi, M. Li, S. Sokhanvaran, and M. Barati. High-temperature refining of metallurgical-grade silicon: A review. *JOM*, Vol. 64, No. 8, 2012, pp. 935–945.
[61] Safarian, J. and M. Tangstad. Vacuum refining of molten silicon. *Metallurgical and Materials Transactions B*, Vol. 43, No. 6, 2012, pp. 1427–1445.
[62] Yasuda, K., K. Morita, and T. H. Okabe. Processes for production of solar-grade silicon using hydrogen reduction and/or thermal decomposition. *Energy Technology*, Vol. 2, No. 2, 2014, pp. 141–154.
[63] Bye, G. and B. Ceccaroli. Solar grade silicon: Technology status and industrial trends. *Solar Energy Materials and Solar Cells*, Vol. 130, 2014, pp. 634–646.
[64] Elwell, D. Electrocrystallization of semiconducting materials from molten salt and organic solutions. *Journal of Crystal Growth*, Vol. 52, 1981, pp. 741–752.
[65] Elwell, D. and R. S. Feigelson. Electrodeposition of solar silicon. *Solar Energy Materials*, Vol. 6, No. 2, 1982, pp. 123–145.
[66] Takeda, Y. and O. Yamamoto. Electrolytic deposition of amorphous silicon. *Denki Kagaku oyobi Kogyo Butsuri Kagaku*, Vol. 52, No. 7, 1984, pp. 460–463.
[67] Fulop, G. F. and R. M. Taylor. Electrodeposition of semiconductors. *Annual Review of Materials Science*, Vol. 15, No. 1, 1985, pp. 197–210.
[68] Elwell, D. and G. M. Rao. Electrolytic production of silicon. *Journal of Applied Electrochemistry*, Vol. 18, No. 1, 1988, pp. 15–22.
[69] Xu, J. and G. M. Haarberg. Electrodeposition of solar cell grade silicon in high temperature molten salts. *High Temperature Materials and Processes*, Vol. 32, 2013, id. 97.
[70] Juzeliūnas, E. and D. J. Fray. Silicon electrochemistry in molten salts. *Chemical Reviews*, Vol. 120, No. 3, 2020, pp. 1690–1709.
[71] Hoopes, W., F. C. Frary, and J. D. Edwards. *Electrolytic refining of aluminum*. U.S. Patent 1,534,318, 1925.
[72] Frary, F. C. The electrolytic refining of aluminum. *Transactions of American Electrochemical Society*, Vol. 47, 1925, pp. 275–286.
[73] Sadoway, D., K. Johansen, B. Myhre, M. Engvoll, and K. Engvoll. Method for electrolytic production and refining of metals. *PCT International Patent*, Vol. WO2007/106709, 2007.
[74] Monnier, R. and J. C. Giacometti. Recherches sur le raffinage électrolytique du silicium. *Helvetica Chimica Acta*, Vol. 47, No. 2, 1964, pp. 345–353.
[75] Monnier, R. and D. Barakat. *Dual cell refining of silicon and germanium*. US Patent, 3,219,561, 1965.
[76] Monnier, R., D. Barakat, and J.-C. Giacometti. *Refining of silicon and germanium*. US Patent, 3,254,010, 1966.
[77] Olson, J. M. and K. L. Carleton. A semipermeable anode for silicon electrorefining. *Journal of the Electrochemical Society*, Vol. 128, No. 12, 1981, pp. 2698–2699.
[78] Sharma, I. G. and T. K. Mukherjee. A study on purification of metallurgical grade silicon by molten salt electrorefining. *Metallurgical Transactions B*, Vol. 17, No. 2, 1986, pp. 395–397.
[79] Lai, Y.-Q., M. Jia, Z.-L. Tian, J. Li, J.-F. Yan, J.-G. Yi, et al. Study on the morphology evolution and purification of electrorefined silicon. *Metallurgical and Materials Transactions A*, Vol. 41, No. 4, 2010, pp. 929–935.
[80] Olsen, E. and S. Rolseth. Three-layer electrorefining of silicon. *Metallurgical and Materials Transactions B*, Vol. 41, No. 2, 2010, pp. 295–302.
[81] Olsen, E., S. Rolseth, and J. Thonstad. Electrocatalytic formation and inactivation of intermetallic compounds in electrorefining of silicon. *Metallurgical and Materials Transactions B*, Vol. 41, No. 4, 2010, pp. 752–757.
[82] Ryu, H. Y., Y. S. An, B. Y. Jang, J. S. Lee, H. H. Nersisyan, M. H. Han, et al. Formation of high purity Si nanofiber from metallurgical grade Si by molten salt electrorefining. *Materials Chemistry and Physics*, Vol. 137, No. 1, 2012, pp. 160–168.
[83] Cai, J., X.-T. Luo, C.-H Lu, G. M. Haarberg, A. Laurent, O. E. Kongstein, et al. Purification of metallurgical grade silicon by electrorefining in molten salts. *Transactions of Nonferrous Metals Society of China*, Vol. 22, No. 12, 2012, pp. 3103–3107.
[84] Cai, J., X.-T. Luo, G. M. Haarberg, O. E. Kongstein, and S.-L. Wang. Electrorefining of metallurgical grade silicon in molten $CaCl_2$ based salts. *Journal of the Electrochemical Society*, Vol. 159, No. 3, 2012, pp. D155–D158.
[85] Zou, X. Y., H. W. Xie, Y. C. Zhai, X. C. Lang, and J. Zhang. Electrolysis process for preparation of solar grade silicon. *Advanced Materials Research*, Vol. 391–392, 2012, pp. 697–702.
[86] Tao, M. Impurity segregation in electrochemical processes and its application to electrorefining of ultrapure silicon. *Electrochimica Acta*, Vol. 89, 2013, pp. 688–691.
[87] De Mattei, R. C., D. Elwell, and R. S. Feigelson. Electrodeposition of silicon at temperatures above its melting point. *Journal of the Electrochemical Society*, Vol. 128, No. 8, 1981, pp. 1712–1714.
[88] De Mattei, R. C., D. Elwell, and R. S. Feigelson. *Electrodeposition of molten silicon*. US Patent, 4,292,145, 1981.
[89] Feigelson, R. S., R. A. Huggins, and D. Elwell. *The electrolytic deposition of low-cost, high-purity polysilicon suitable for use in solar-cell devises DOE Report, DOE/ER/70067-T70061*, 1982.

[90] Cohen, U. and R. A. Huggins. Silicon epitaxial growth by electrodeposition from molten fluorides. *Journal of the Electrochemical Society*, Vol. 123, No. 3, 1976, pp. 381–383.
[91] Cohen, U. *Epitaxial growth of silicon or germanium by electrodeposition from molten salts*. US Patent, 3,983,012, 1976.
[92] Cohen, U. *Electrodeposition of polycrystalline silicon from a molten fluoride bath and product*. US Patent, 4,142,947, 1979.
[93] Rao, G. M., D. Elwell, and R. S. Feigelson. Electrowinning of silicon from K_2SiF_6 - molten fluoride systems. *Journal of the Electrochemical Society*, Vol. 127, No. 9, 1980, pp. 1940–1944.
[94] Rao, G. M., D. Elwell, and R. S. Feigelson. Electrocoating of silicon and its dependence on the time of electrolysis. *Surface Technology*, Vol. 13, No. 4, 1981, pp. 331–337.
[95] Rao, G. M., D. Elwell, and R. S. Feigelson. Electrodeposition of silicon onto graphite. *Journal of the Electrochemical Society*, Vol. 128, No. 8, 1981, pp. 1708–1711.
[96] Elwell, D. and G. M. Rao. Mechanism of electrodeposition of silicon from K_2SiF_6-flinak. *Electrochimica Acta*, Vol. 27, No. 6, 1982, pp. 673–676.
[97] Rao, G. M., D. Elwell, and R. S. Feigelson. Characterization of electrodeposited silicon on graphite. *Solar Energy Materials*, Vol. 7, No. 1, 1982, pp. 15–21.
[98] Elwell, D., R. S. Feigelson, and G. M. Rao. The morphology of silicon electrodeposits on graphite substrates. *Journal of the Electrochemical Society*, Vol. 130, No. 5, 1983, pp. 1021–1025.
[99] Elwell, D. and G. M. Rao. Time dependence of cell voltage during electrolysis of K_2SiF_6-KF-LiF melts. *Surface Technology*, Vol. 23, No. 1, 1984, pp. 67–72.
[100] Elwell, D. Electrowinning of silicon from solutions of silica in alkali metal fluoride/alkaline earth fluoride eutectics. *Solar Energy Materials*, Vol. 5, No. 2, 1981, pp. 205–210.
[101] Boiko, O. I., Y. K. Delimarskii, and R. V. Chermov. Conditions for production of powdered silicon by electrolysis of fluoride-oxide melts. *Poroshkovaya Metallurgiya* (*Kiev*), Vol. 6, 1982, pp. 1–4.
[102] Boiko, O. I., Y. K. Delimarskii, and R. V. Chernov. Conditions for production of powdered silicon by electrolysis of fluoride-oxide melts. *Soviet Powder Metallurgy and Metal Ceramics* (*English translation of Poroshk Metall* (*Kiev*)), Vol. 21, No. 6, 1982, pp. 425–427.
[103] Carleton, K. L., J. M. Olson, and A. Kibbler. Electrochemical nucleation and growth of silicon in molten fluorides. *Journal of the Electrochemical Society*, Vol. 130, No. 4, 1983, pp. 782–786.
[104] Boen, R. and J. Bouteillon. The electrodeposition of silicon in fluoride melts. *Journal of Applied Electrochemistry*, Vol. 13, No. 3, 1983, pp. 277–288.
[105] Lepinay, J. de., J. Bouteillon, S. Traore, D. Renaud, and M. J. Barbier. Electroplating silicon and titanium in molten fluoride media. *Journal of Applied Electrochemistry*, Vol. 17, No. 2, 1987, pp. 294–302.
[106] Stern, K. H. and M. E. McCollum. Electrodeposition of silicon from molten salts. *Thin Solid Films*, Vol. 124, No. 2, 1985, pp. 129–134.
[107] Prutskov, D. V., A. A. Andriiko, Y. K. Delimarskii, and R. V. Chernov. Electroreduction of silicon compounds in the sodium hexafluoroaluminate-aluminum trifluoride-silica melt. *Ukr Khim Zh* (*Russ Ed*), Vol. 51, No. 8, 1985, pp. 826–830.
[108] Moore, J. T., T. H. Wang, M. J. Heben, K. Douglas, and T. F. Ciszek. Fused-salt electrodeposition of thin-layer silicon. *Conference Record of the Twenty Sixth IEEE Photovoltaic Specialists Conference – 1997*, 1997, pp. 775–778.
[109] Saegusa, K., T. Oishi, and K. Koyama. *Method for producing silicon*. PCT International Patent, WO 2007/139023, 2007.
[110] Saegusa, K., T. Oishi, and K. Koyama. *Method for producing purified metal and semimetal*. Japanese Patent, JPA2011006317, 2011.
[111] Oishi, T., M. Watanabe, K. Koyama, M. Tanaka, and K. Saegusa. Process for solar grade silicon production by molten salt electrolysis using aluminum-silicon liquid alloy. *Journal of the Electrochemical Society*, Vol. 158, No. 9, 2011, pp. E93–E99.
[112] Osen, K. S., A. M. Martinez, S. Rolseth, H. Gudbrandsen, M. Juel, and G. M. Haarberg. Electrodeposition of crystalline silicon films from alkali fluoride mixtures. *ECS Transactions*, Vol. 33, No. 7, 2010, pp. 429–438.
[113] Haarberg, G. M., L. Famiyeh, A. M. Martinez, and K. S. Osen. Electrodeposition of silicon from fluoride melts. *Electrochimica Acta*, Vol. 100, 2013, pp. 226–228.
[114] Zongying, C., Y. Li, and W. Tian. Electrochemical behavior of silicon compound in LiF-NaF-KF-Na_2SiF_6 molten salt. *Ionics*, Vol. 17, 2011, pp. 821–826.
[115] Abbar, A. H., S. H. Kareem, and F. A. Alsaady. Electrodeposition of silicon from fluorosilicic acid produced in Iraqi phosphate fertilizer plant. *Journal of Electrochemical Science and Technology*, Vol. 2, No. 3, 2011, pp. 168–173.
[116] Bieber, A. L., L. Massot, M. Gibilaro, L. Cassayre, P. Chamelot, and P. Taxil. Fluoroacidity evaluation in molten salts. *Electrochimica Acta*, Vol. 56, No. 14, 2011, pp. 5022–5027.
[117] Bieber, A. L., L. Massot, M. Gibilaro, L. Cassayre, P. Taxil, and P. Chamelot. Silicon electrodeposition in molten fluorides. *Electrochimica Acta*, Vol. 62, 2012, pp. 282–289.
[118] Hu, Y., X. Wang, J. Xiao, J. Hou, S. Jiao, and H. Zhu. Electrochemical behavior of silicon(IV) ion in BaF_2-CaF_2-SiO_2 melts at 1,573K. *Journal of the Electrochemical Society*, Vol. 160, No. 3, 2013, pp. D81–D84.
[119] Sakanaka, Y. and T. Goto. Electrodeposition of Si film on Ag substrate in molten LiF–NaF–KF directly dissolving SiO_2. *Electrochimica Acta*, Vol. 164, 2015, pp. 139–142.
[120] Suzuki, Y., Y. Inoue, M. Yokota, and T. Goto. Effects of oxide ions on the electrodeposition process of silicon in molten fluorides. *Journal of the Electrochemical Society*, Vol. 166, No. 13, 2019, pp. D564–D568.
[121] Stern, D. R. and Q. H. Mckenna. *Production of pure elemental silicon*. US Patent, 2,892,763, 1959.
[122] Matsuda, T., S. Nakamura, K.-I. Ide, K. Nyudo, S. Yae, and Y. Nakato. Oscillatory behavior in electrochemical deposition reaction of polycrystalline silicon thin films through reduction of silicon tetrachloride in a molten salt electrolyte. *Chemistry Letters*, Vol. 25, No. 7, 1996, pp. 569–570.
[123] Kongstein, O. E., C. Wollan, S. Sultana, and G. M. Haarberg. Electrorefining of silicon in molten calcium chloride. *ECS Transactions*, Vol. 3, No. 35, 2007, pp. 357–361.
[124] Sakanaka, Y., A. Murata, T. Goto, and K. Hachiya. Electrodeposition of porous Si film from SiO_2 in molten

$BaCl_2$-$CaCl_2$-NaCl. *Journal of Alloys and Compounds*, Vol. 695, 2017, pp. 2131–2135.

[125] Yang, X., L. Ji, X. Zou, T. Lim, J. Zhao, E. T. Yu, et al. Toward cost-effective manufacturing of silicon solar cells: electrodeposition of high-quality si films in a $CaCl_2$-based molten salt. *Angewandte Chemie International Edition*, Vol. 56, No. 47, 2017, pp. 15078–15082.

[126] Zou, X., L. Ji, X. Yang, T. Lim, E. T. Yu, and A. J. Bard. Electrochemical formation of a p–n junction on thin film silicon deposited in molten salt. *Journal of the American Chemical Society*, Vol. 139, No. 45, 2017, pp. 16060–16063.

[127] Zou, X., L. Ji, J. Ge, D. R. Sadoway, E. T. Yu, and A. J. Bard. Electrodeposition of crystalline silicon films from silicon dioxide for low-cost photovoltaic applications. *Nature Communications*, Vol. 10, No. 1, 2019, id. 5772.

[128] Weng, W. and W. Xiao. Electrodeposited silicon nanowires from silica dissolved in molten salts as a binder-free anode for lithium-ion batteries. *ACS Applied Energy Materials*, Vol. 2, No. 1, 2019, pp. 804–813.

[129] Pangarov, N. and I. V. Tomov. X-ray structure determination of the axis of preferred orientation of twin crystals in a textured metallic layer. *Izv Bolgarskoi Akad Nauk Ser Khim*, Vol. 2, No. 4, 1969, id. 819.

[130] Delimarskii, Y. K., N. N. Storchak, and R. V. Chermov. Electrodeposition of silicon on solid electrodes. *Elektrokhimiya*, Vol. 9, No. 10, 1973, pp. 1443–1447.

[131] Delimarskii, Y. K., N. Storchak, and R. V. Chermov. Electrodeposition of silicon on solid electrodes. *Soviet Electrochemistry*, Vol. 9, No. 10, 1973, pp. 1362–1365.

[132] Boiko, O. I., Y. K. Delimarskii, and R. V. Chernov. Electrochemical reduction of silicon(IV) from a fluoride-chloride melt. *Ukr Khim Zh* (*Russ Ed*), Vol. 51, No. 4, 1985, pp. 385–390.

[133] Frolenco, D. B., Z. S. Martem'yanova, Z. I. Valeev, and A. N. Baraboshkin. Structure of silicon deposits obtained by electrolyzing mixed chloride-fluoride melts. *Soviet Electrochemistry* (*English translation of Electrokhimiya*), Vol. 28, No. 12, 1992, pp. 1427–1434.

[134] Frolenko, D. B., Z. S. Martem'yanova, A. N. Baraboshkin, and S. V. Plaksin. Electrodeposition of silicon from fluoride-chloride melts. *Melts* (*English translation of Rasplavy*), Vol. 7, No. 5, 1993, pp. 308–314.

[135] Zaykov, Y. uP., A. V. Isakov, A. P. Apisarov, and O. V. Chemezov. Production of silicon by electrolysis of halide and oxide-halide melts. *Tsveynye Metally*, Vol. 12, 2013, pp. 58–62.

[136] Zaykov, Y. P., S. I. Zhuk, A. V. Isakov, O. V. Grishenkova, and V. A. Isaev. Electrochemical nucleation and growth of silicon in the KF-KCl-K_2SiF_6 melt. *Journal of Solid State Electrochemistry*, Vol. 19, No. 5, 2015, pp. 1341–1345.

[137] Zhuk, S. I., V. A. Isaev, O. V. Grishenkova, A. V. Isakov, A. P. Apisarov, and Y. P. Zaikov. Silicon electrodeposition from chloride-fluoride melts containing K_2SiF_6 and SiO_2. *Journal of the Serbian Chemical Society*, Vol. 81, No. 1, 2017, pp. 51–62.

[138] Zhuk, S. I., A. V. Isakov, A. P. Apisarov, O. V. Grishenkova, V. A. Isaev, E. G. Vovkotrub, et al. Electrodeposition of continuous silicon coatings from the KF-KCl-K_2SiF_6 melts. *Journal of the Electrochemical Society*, Vol. 164, No. 8, 2017, pp. H5135–H5138.

[139] Laptev, M. V., A. V. Isakov, O. V. Grishenkova, A. S. Vorob'ev, A. O. Khudorozhkova, L. A. Akashev, et al. Electrodeposition of thin silicon films from the KF-KCl-KI-K_2SiF_6 Melt. *Journal of the Electrochemical Society*, Vol. 167, No. 4, 2020, id. 042506.

[140] Isakov, A., S. Khvostov, E. Kinev, M. Laptev, A. Khudorozhkova, O. Grishenkova, et al. Neutron transmutation doping of thin silicon films electrodeposited from the KF-KCl-KI-K_2SiF_6 melt. *Journal of the Electrochemical Society*, Vol. 167, No. 8, 2020, id. 082515.

[141] Zaykov, Y. P., A. V. Isakov, I. D. Zakiryanova, O. G. Reznitskikh, O. V. Chemezov, and A. A. Redkin. Interaction between SiO_2 and a KF–KCl–K_2SiF_6 Melt. *The Journal of Physical Chemistry B*, Vol. 118, No. 6, 2014, pp. 1584–1588.

[142] Kuznetsova, S. V., V. S. Dolmatov, and S. A. Kuznetsov. Voltammetric study of electroreduction of silicon complexes in a chloride-fluoride melt. *Russian Journal of Electrochemistry*, Vol. 45, No. 7, 2009, pp. 742–748.

[143] Maeda, K., K. Yasuda, T. Nohira, R. Hagiwara, and T. Homma. Silicon electrodeposition in water-soluble KF–KCl molten salt: investigations on the reduction of Si(IV) ions. *Journal of the Electrochemical Society*, Vol. 162, No. 9, 2015, pp. D444–D448.

[144] Yasuda, K., K. Maeda, T. Nohira, R. Hagiwara, and T. Homma. Silicon electrodeposition in water-soluble KF–KCl molten salt: Optimization of electrolysis conditions at 923 K. *Journal of the Electrochemical Society*, Vol. 163, No. 3, 2016, pp. D95–D99.

[145] Yasuda, K., K. Saeki, T. Kato, R. Hagiwara, and T. Nohira. Silicon electrodeposition in a water-soluble KF–KCl molten salt: effects of temperature and current density. *Journal of the Electrochemical Society*, Vol. 165, No. 16, 2018, pp. D825–D831.

[146] Yasuda, K., K. Maeda, R. Hagiwara, T. Homma, and T. Nohira. Silicon Electrodeposition in a water-Soluble KF–KCl molten salt: Utilization of $SiCl_4$ as Si source. *Journal of the Electrochemical Society*, Vol. 164, No. 2, 2017, pp. D67–D71.

[147] Peng, J., H. Yin, J. Zhao, X. Yang, A. J. Bard, and D. R. Sadoway. Liquid-tin-assisted molten salt electrodeposition of photoresponsive n-type silicon films. *Advanced Functional Materials*, Vol. 28, No. 1, 2018, id. 1703551.

[148] Haarberg, G. M., T. Kato, Y. Norikawa, and T. Nohira. Electrodeposition of silicon with a liquid gallium cathode in molten salts. *ECS Transactions*, Vol. 89, No. 7, 2019, pp. 29–35.

[149] Katayama, Y., M. Yokomizo, T. Miura, and T. Kishi. Preparation of a novel fluorosilicate salt for electrodeposition of silicon at low temperature. *Electrochemistry*, Vol. 69, No. 11, 2001, pp. 834–836.

[150] Abedin, S. Z. E., N. Borissenko, and F. Endres. Electrodeposition of nanoscale silicon in a room temperature ionic liquid. *Electrochemistry Communications*, Vol. 6, No. 5, 2004, pp. 510–514.

[151] Borisenko, N., S. Z. E. Abedin, and F. Endres. *In situ* STM investigation of gold reconstruction and of silicon electrodeposition on Au(111) in the room temperature ionic liquid 1-butyl-1-methylpyrrolidinium bis(trifluoromethylsulfonyl) imide. *The Journal of Physical Chemistry B*, Vol. 110, No. 12, 2006, pp. 6250–6256.

[152] Al-Salman, R., S. Z. El Abedin, and F. Endres. Electrodeposition of Ge, Si and Si_xGe_{1-x} from an air- and water-stable ionic liquid. *Physical Chemistry Chemical Physics*, Vol. 10, No. 31, 2008, pp. 4650–4657.
[153] Nishimura, Y., Y. Fukunaka, T. Nishida, T. Nohira, and R. Hagiwara. Electrodeposition of Si thin film in a hydrophobic room-temperature molten salt. *Electrochemical and Solid-State Letters*, Vol. 11, No. 9, 2008, pp. D75–D79.
[154] Nishimura, Y., T. Nohira, T. Morioka, and R. Hagiwara. Electrochemical reduction of silicon tetrachloride in an intermediate-temperature ionic liquid. *Electrochemistry*, Vol. 77, No. 8, 2009, pp. 683–686.
[155] Martinez, A. M., K. S. Osen, O. E. Kongstein, E. Sheridan, A. G. Ulyashin, and G. M. Haarberg. Electrodeposition of silicon thin films from ionic liquids. *ECS Transactions*, Vol. 25, No. 27, 2010, pp. 107–118.
[156] Fournier, C. and F. Favier. Zn, Ti and Si nanowires by electrodeposition in ionic liquid. *Electrochemistry Communications*, Vol. 13, No. 11, 2011, pp. 1252–1255.
[157] Komadina, J., T. Akiyoshi, Y. Ishibashi, Y. Fukunaka, and T. Homma. Electrochemical quartz crystal microbalance study of Si electrodeposition in ionic liquid. *Electrochimica Acta*, Vol. 100, 2013, pp. 236–241.
[158] Tsuyuki, Y., T. A. P. Huynh, J. Komadina, Y. Fukunaka, and T. Homma. Electrochemical quartz crystal microbalance, X-ray photoelectron spectroscopy, and Raman spectroscopy analysis of $SiCl_4$ reduction in ionic liquids. *Electrochimica Acta*, Vol. 183, 2015, pp. 49–55.
[159] Tsuyuki, Y., T. Fujimura, M. Kunimoto, Y. Fukunaka, P. Pianetta, and T. Homma. Analysis of cathodic reaction process of $SiCl_4$ during Si electrodeposition in ionic liquids. *Journal of the Electrochemical Society*, Vol. 164, No. 14, 2017, pp. D994–D998.
[160] Tsuyuki, Y., H. Takai, Y. Fukunaka, and T. Homma. Formation of Si thin films by electrodeposition in ionic liquids for solar cell applications. *Japanese Journal of Applied Physics*, Vol. 57, No. 8S3, 2018, id. 08RB11.
[161] Pulletikurthi, G., A. Lahiri, T. Carstens, N. Borisenko, S. Z. E. Abedin, and F. Endres. Electrodeposition of silicon from three different ionic liquids: possible influence of the anion on the deposition process. *Journal of Solid State Electrochemistry*, Vol. 17, No. 11, 2013, pp. 2823–2832.
[162] Park, J., C. K. Lee, K. Kwon, and H. Kim. Electrodeposition of silicon from 1-butyl-3-methylpyridinium bis(trifluromethylsulfonyl) imide ionic liquid. *International Journal of Electrochemical Science*, Vol. 8, No. 3, 2013, pp. 4206–4214.
[163] Zhang, J., S. Chen, H. Zhang, S. Zhang, X. Yao, and Z. Shi. Electrodeposition of crystalline silicon directly from silicon tetrachloride in ionic liquid at low temperature. *RSC Advances*, Vol. 6, No. 15, 2016, pp. 12061–12067.
[164] Shah, N. K., R. K. Pati, A. Ray, and I. Mukhopadhyay. Electrodeposition of Si from an ionic liquid bath at room temperature in the presence of water. *Langmuir*, Vol. 33, No. 7, 2017, pp. 1599–1604.
[165] Thomas, S., D. Kowalski, M. Molinari, and J. Mallet. Role of electrochemical process parameters on the electrodeposition of silicon from 1-butyl-1-methylpyrrolidinium bis(trifluoromethanesulfonyl)imide ionic liquid. *Electrochimica Acta*, Vol. 265, 2018, pp. 166–174.
[166] Zhao, Z., J. Liu, and C. Zhang. Preparation and characterization of electrochemically deposited silicon films in ionic liquid from polysilicon byproduct SiCl. *International Journal of Electrochemical Science*, Vol. 13, No. 9, 2018, pp. 8766–8774.
[167] Zhao, Z., C. Yang, L. Wu, C. Zhang, R. Wang, and E. Ma. Preparation and characterization of crystalline silicon by electrochemical liquid–liquid–solid crystal growth in ionic liquid. *ACS Omega*, Vol. 6, No. 18, 2021, pp. 11935–11942.
[168] Zyazev, Y. A. and A. I. Ezrielev. Possible electrolytic preparations of silicon. *Sb Tr Agron Fiz*, 13, 1966, pp. 32–38.
[169] Austin, A. E. *Silicon electrodeposition*. US Patent, 3,990,953, 1976.
[170] Austin, A. E., A. K. Agrawal, and G. T. Noel. *DOE Report, DOE/ET/2052C4*, 1979.
[171] Agrawal, A. K. and A. E. Austin. Electrodeposition of silicon from solutions of silicon halides in aprotic solvents. *Journal of the Electrochemical Society*, Vol. 128, No. 11, 1981, pp. 2292–2296.
[172] Kröger, F. A. *Low cost solar cells based on amorphous silicon electrodeposited from organic solvents DOE Report, SAN-0113-040-T6*, 1980.
[173] Lee, C. H. and F. A. Kröger. Cathodic deposition of amorphous alloys of silicon, carbon, and fluorine. *Journal of the Electrochemical Society*, Vol. 129, No. 5, 1982, pp. 936–942.
[174] Mohan, T. R. R. and F. A. Kröger. Cathodic deposition of amorphous silicon from solutions of silicic acid and tetraethyl ortho-silicate in ethylene glycol and formamide containing HF. *Electrochimica Acta*, Vol. 27, No. 3, 1982, pp. 371–377.
[175] Takeda, Y., R. Kanno, O. Yamamoto, T. R. R. Mohan, C. H. Lee, and F. A. Kröger. Cathodic deposition of amorphous silicon from tetraethylorthosilicate in organic solvents. *Journal of the Electrochemical Society*, Vol. 128, No. 6, 1981, pp. 1221–1224.
[176] Gobet, J. and H. Tannenberger. Electrodeposition of silicon from a nonaqueous solvent. *Journal of the Electrochemical Society*, Vol. 135, No. 1, 1988, pp. 109–112.
[177] Sarma, P. R. L., T. R. R. Mohan, S. Venkatachalam, J. Singh, and V. P. Sundersingh. Structural and morphological studies of electrodeposited amorphous silicon thin films. *Materials Science and Engineering: B*, Vol. 15, No. 3, 1992, pp. 237–243.
[178] Ram, P., J. Singh, T. R. Ramamohan, S. Venkatachalam, and V. P. Sundarsingh. Surface properties of electrodeposited a-Si:C:H:F thin films by X-ray photoelectron spectroscopy. *Journal of Materials Science*, Vol. 32, No. 23, 1997, pp. 6305–6310.
[179] Nicholson, J. P. Electrodeposition of silicon from nonaqueous solvents. *Journal of the Electrochemical Society*, Vol. 152, No. 12, 2005, pp. C795–C802.
[180] Nishimura, Y. and Y. Fukunaka. Electrochemical reduction of silicon chloride in a non-aqueous solvent. *Electrochimica Acta*, Vol. 53, No. 1, 2007, pp. 111–116.
[181] Ma, Q. P., W. Liu, B. C. Wang, and Q. S. Meng. Electrodeposition of silicon in organic solvent containing silicon chloride. *Advanced Materials Research*, Vol. 79–82, 2009, pp. 1635–1638.
[182] Munisamy, T. and A. J. Bard. Electrodeposition of Si from organic solvents and studies related to initial stages of Si

growth. *Electrochimica Acta*, Vol. 55, No. 11, 2010, pp. 3797–3803.

[183] Epur, R., M. Ramanathan, F. R. Beck, A. Manivannan, and P. N. Kumta. Electrodeposition of amorphous silicon anode for lithium ion batteries. *Materials Science and Engineering: B*, Vol. 177, No. 14, 2012, pp. 1157–1162.

[184] Zhao, G., Y. Meng, N. Zhang, and K. Sun. Electrodeposited Si film with excellent stability and high rate performance for lithium-ion battery anodes. *Materials Letters*, Vol. 76, 2012, pp. 55–58.

[185] Bechelany, M., J. Elias, P. Brodard, J. Michler, and L. Philippe. Electrodeposition of amorphous silicon in non-oxygenated organic solvent. *Thin Solid Films*, Vol. 520, No. 6, 2012, pp. 1895–1901.

[186] Vichery, C., V. Le Nader, C. Frantz, Y. Zhang, J. Michler, and L. Philippe. Stabilization mechanism of electrodeposited silicon thin films. *Physical Chemistry Chemical Physics*, Vol. 16, No. 40, 2014, pp. 22222–22228.

[187] Gu, J., E. Fahrenkrug, and S. Maldonado. Direct electrodeposition of crystalline silicon at low temperatures. *Journal of the American Chemical Society*, Vol. 135, No. 5, 2013, pp. 1684–1687.

[188] Abbar, A. H. and S. H. Kareem. Cathodic deposition of silicon from phenyltrichlorosilane in an organic solvent. *International Journal of Electrochemical Science*, Vol. 8, 2013, pp. 10650–10659.

[189] Krywko-Cendrowska, A., L. Marot, M. Strawski, R. Steiner, and E. Meyer. Electrodeposition and characterization of SiO_x films photoactive in organic solution. *Journal of the Electrochemical Society*, Vol. 163, No. 3, 2016, pp. D100–D106.

[190] Gattu, B., R. Epur, P. Shanti, P. Jampani, R. Kuruba, M. Datta, et al. Pulsed current electrodeposition of silicon thin films anodes for lithium ion battery applications. *Inorganics*, Vol. 5, No. 2, 2017, id. 27.

[191] Oki, T. and H. Inoue. Reduction of titanium dioxide by calcium in a hot cathode spot. *Memoirs of the Faculty of Engineering, Nagoya University*, Vol. 19, No. 1, 1967, pp. 164–166.

[192] Okabe, T. H., I. Park, K. T. Jacob, and Y. Waseda. Production of niobium powder by electronically mediated reaction (EMR) using calcium as a reductant. *Journal of Alloys and Compounds*, Vol. 288, No. 1–2, 1999, pp. 200–210.

[193] Chen, G. Z., D. J. Fray, and T. W. Farthing. Direct electrochemical reduction of titanium dioxide to titanium in molten calcium chloride. *Nature* (*London*), Vol. 407, No. 6802, 2000, pp. 361–364.

[194] Sharma, R. A. *Metallothermic reduction of rare earth oxides*. US Patent, US 4,578,242, 1986.

[195] Sharma, R. A. and R. N. Seefurth. Metallothermic reduction of neodymium sesquioxide with calcium in calcium chloride-sodium chloride melts. *Journal of the Electrochemical Society*, Vol. 135, No. 1, 1988, pp. 66–71.

[196] Kipouros, G. J. and R. A. Sharma. Electrolytic regeneration of the neodymium oxide reduction-spent salt. *Journal of the Electrochemical Society*, Vol. 137, No. 11, 1990, pp. 3333–3338.

[197] Ono, K. and R. Suzuki. A new concept for producing Ti sponge: Calciothermic reduction. *JOM*, Vol. 54, No. 2, 2002, pp. 59–61.

[198] Wang, D., X. Jin, and G. Z. Chen. Solid state reactions: an electrochemical approach in molten salts. *Annual Reports on the Progress of Chemistry, Section C*, Vol. 104, 2008, pp. 189–234.

[199] Abdelkader, A. M., K. T. Kilby, A. Cox, and D. J. Fray. DC voltammetry of electro-deoxidation of solid oxides. *Chemical Review* (*Washington, DC, US*), Vol. 113, No. 5, 2013, pp. 2863–2886.

[200] Xiao, W. and D. Wang. The electrochemical reduction processes of solid compounds in high temperature molten salts. *Chemical Society Reviews*, Vol. 43, No. 10, 2014, pp. 3215–3228.

[201] Nohira, T., K. Yasuda, and Y. Ito. Pinpoint and bulk electrochemical reduction of insulating silicon dioxide to silicon. *Nature Materials*, Vol. 2, No. 6, 2003, pp. 397–401.

[202] Yasuda, K., T. Nohira, and Y. Ito. Effect of electrolysis potential on reduction of solid silicon dioxide in molten $CaCl_2$. *Journal of Physics and Chemistry of Solids*, Vol. 66, No. 2–4, 2005, pp. 443–447.

[203] Yasuda, K., T. Nohira, K. Amezawa, Y. H. Ogata, and Y. Ito. Mechanism of direct electrolytic reduction of solid SiO_2 to Si in molten $CaCl_2$. *Journal of the Electrochemical Society*, Vol. 152, No. 4, 2005, pp. D69–D74.

[204] Yasuda, K., T. Nohira, R. Hagiwara, and Y. H. Ogata. Direct electrolytic reduction of solid SiO_2 in molten $CaCl_2$ for the production of solar grade silicon. *Electrochimica Acta*, Vol. 53, No. 1, 2007, pp. 106–110.

[205] Yasuda, K., T. Nohira, R. Hagiwara, and Y. H. Ogata. Diagrammatic representation of direct electrolytic reduction of SiO_2 in molten $CaCl_2$. *Journal of the Electrochemical Society*, Vol. 154, No. 7, 2007, pp. E95–E101.

[206] Nohira, T., N. Kani, T. Tsuda, and R. Hagiwara. Electrolytic reduction of solid SiO_2 in molten $CaCl_2$ for the production of solar-grade silicon. *ECS Transactions*, Vol. 16, No. 49, 2009, pp. 239–245.

[207] Nohira, T. Direct electrolytic reduction from silica to silicon in molten salts. *Yoyuen Oyobi Koon Kagaku*, Vol. 54, No. 3, 2011, pp. 95–103.

[208] Yasuda, K., T. Nohira, K. Kobayashi, N. Kani, T. Tsuda, and R. Hagiwara. Improving purity and process volume during direct electrolytic reduction of solid SiO_2 in molten $CaCl_2$ for the production of solar-grade silicon. *Energy Technology* (*Weinheim, Ger*), Vol. 1, No. 4, 2013, pp. 245–252.

[209] Jin, X., P. Gao, D. Wang, X. Hu, and G. Z. Chen. Electrochemical preparation of silicon and its alloys from solid oxides in molten calcium chloride. *Angewandte Chemie International Edition*, Vol. 43, No. 6, 2004, pp. 733–736.

[210] Deng, Y., D. Wang, W. Xiao, X. Jin, X. Hu, and G. Z. Chen. Electrochemistry at conductor/insulator/electrolyte three-phase interlines: A thin layer model. *The Journal of Physical Chemistry B*, Vol. 109, No. 29, 2005, pp. 14043–14051.

[211] Xiao, W., X. Jin, Y. Deng, D. Wang, and G. Z. Chen. Rationalisation and optimisation of solid state electro-reduction of SiO_2 to Si in molten $CaCl_2$ in accordance with dynamic three-phase interlines based voltammetry. *The Journal of Electroanalytical Chemistry*, Vol. 639, No. 1–2, 2010, pp. 130–140.

[212] Xiao, W., X. Jin, Y. Deng, D. Wang, X. Hu, and G. Z. Chen. Electrochemically driven three-phase interlines into insulator

compounds: electroreduction of solid SiO_2 in molten $CaCl_2$. *ChemPhysChem*, Vol. 7, No. 8, 2006, pp. 1750–1758.

[213] Xiao, W., X. Jin, and G. Z. Chen. Up-scalable and controllable electrolytic production of photo-responsive nanostructured silicon. *Journal of Materials Chemistry A*, Vol. 1, No. 35, 2013, pp. 10243–10250.

[214] Yasuda, K., T. Nohira, Y. H. Ogata, and Y. Ito. Direct electrolytic reduction of solid silicon dioxide in molten LiCl-KCl-$CaCl_2$ at 773 K. *Journal of the Electrochemical Society*, Vol. 152, No. 11, 2005, pp. D208–D212.

[215] Kobayashi, K., T. Nohira, R. Hagiwara, K. Ichitsubo, and K. Yamada. Direct electrolytic reduction of powdery SiO_2 in molten $CaCl_2$ with pellet-type SiO_2 contacting electrodes. *ECS Transactions*, Vol. 33, No. 7, 2010, pp. 239–248.

[216] Nishimura, Y., T. Nohira, K. Yasuda, Y. Fukunaka, and R. Hagiwara. Direct electrolytic reduction of amorphous SiO_2 powder refined from diatomaceous earth. *Transactions of the Materials Research Society of Japan*, Vol. 35, No. 1, 2010, pp. 47–49.

[217] Nishimura, Y., T. Nohira, K. Kobayashi, and R. Hagiwara. Formation of Si nanowires by direct electrolytic reduction of porous SiO_2 pellets in molten $CaCl_2$. *Journal of the Electrochemical Society*, Vol. 158, No. 6, 2011, pp. E55–E59.

[218] Xiao, W., X. Wang, H. Yin, H. Zhu, X. Mao, and D. Wang. Verification and implications of the dissolution-electrodeposition process during the electro-reduction of solid silica in molten $CaCl_2$. *RSC Advances*, Vol. 2, No. 19, 2012, pp. 7588–7593.

[219] Pistorius, P. C. and D. J. Fray. Formation of silicon by electrodeoxidation, and implications for titanium metal production. *Journal of the Southern African Institute of Mining and Metallurgy*, Vol. 106, No. 1, 2006, pp. 31–41.

[220] Lee, S.-C., J.-M. Hur, and C.-S. Seo. Silicon powder production by electrochemical reduction of SiO_2 in molten LiCl–Li_2O. *Journal of Industrial and Engineering Chemistry*, Vol. 14, No. 5, 2008, pp. 651–654.

[221] Yang, J., S. Lu, S. Kan, X. Zhang, and J. Du. Electrochemical preparation of silicon nanowires from nanometer silica in molten calcium chloride. *Chemical Communications* (*Cambridge, U K*), Vol. 22, 2009, pp. 3273–3275.

[222] Juzeliunas, E., A. Cox, and D. J. Fray. Silicon surface texturing by electro-deoxidation of a thin silica layer in molten salt. *Electrochemistry Communications*, Vol. 12, No. 10, 2010, pp. 1270–1274.

[223] Juzeliunas, E., A. Cox, and D. J. Fray. Electro-deoxidation of thin silica layer in molten salt – Globular structures with effective light absorbance. *Electrochimica Acta*, Vol. 68, 2012, pp. 123–127.

[224] Ergül, E., İ. Karakaya, and M. Erdoğan. Electrochemical decomposition of SiO_2 pellets to form silicon in molten salts. *Journal of Alloys and Compounds*, Vol. 509, No. 3, 2011, pp. 899–903.

[225] Cho, S. K., F.-R. F. Fan, and A. J. Bard. Formation of a silicon layer by electroreduction of SiO_2 nanoparticles in $CaCl_2$ molten salt. *Electrochimica Acta*, Vol. 65, No. 0, 2012, pp. 57–63.

[226] Cho, S. K., F.-R. F. Fan, and A. J. Bard. Electrodeposition of crystalline and photoactive silicon directly from silicon dioxide nanoparticles in molten $CaCl_2$. *Angewandte Chemie International Edition*, Vol. 51, No. 51, 2012, pp. 12740–12744.

[227] Zhao, J., H. Yin, T. Lim, H. Xie, H.-Y. Hsu, F. Forouzan, et al. Electrodeposition of photoactive silicon films for low-cost solar cells. *Journal of the Electrochemical Society*, Vol. 163, No. 9, 2016, pp. D506–D514.

[228] Toba, T., K. Yasuda, T. Nohira, X. Yang, R. Hagiwara, K. Ichitsubo, et al. Electrolytic reduction of SiO_2 granules in molten $CaCl_2$. *Electrochemistry* (*Tokyo, Jpn*), Vol. 81, No. 7, 2013, pp. 559–565.

[229] Yang, X., K. Yasuda, T. Nohira, R. Hagiwara, and T. Homma. Reaction behavior of stratified SiO_2 granules during electrochemical reduction in molten $CaCl_2$. *Metallurgical and Materials Transactions B*, Vol. 45, No. 4, 2014, pp. 1337–1344.

[230] Yang, X., K. Yasuda, T. Nohira, R. Hagiwara, and T. Homma. Kinetic characteristics of electrochemical reduction of SiO_2 granules in molten $CaCl_2$. *Journal of the Electrochemical Society*, Vol. 161, No. 7, 2014, pp. D3116–D3119.

[231] Yang, X., K. Yasuda, T. Nohira, R. Hagiwara, and T. Homma. The role of granule size on the kinetics of electrochemical reduction of SiO_2 granules in molten $CaCl_2$. *Metallurgical and Materials Transactions B*, Vol. 47, No. 1, 2016, pp. 788–797.

[232] Yang, X., K. Yasuda, T. Nohira, R. Hagiwara, and T. Homma. Cathodic potential dependence of electrochemical reduction of SiO_2 granules in molten $CaCl_2$. *Metallurgical and Materials Transactions E*, Vol. 3, No. 3, 2016, pp. 145–155.

[233] Zhao, J., J. Li, P. Ying, W. Zhang, L. Meng, and C. Li. Facile synthesis of freestanding Si nanowire arrays by one-step template-free electro-deoxidation of SiO_2 in a molten salt. *Chemical Communications* (*Cambridge, UK*), Vol. 49, No. 40, 2013, pp. 4477–4479.

[234] Yasuda, K. Development of electrolytic production process of silicon utilizing liquid Zn alloy. *Yoyuen Oyobi Koon Kagaku*, Vol. 58, No. 1, 2015, pp. 20–27.

[235] Yasuda, K., T. Shimao, R. Hagiwara, T. Homma, and T. Nohira. Electrolytic production of silicon using liquid zinc alloy in molten $CaCl_2$. *Journal of the Electrochemical Society*, Vol. 164, No. 8, 2017, pp. H5049–H5056.

[236] Islam, M. M., I. Abdellaoui, C. Moslah, T. Sakurai, M. Ksibi, S. Hamzaoui, et al. Electrodeposition and characterization of silicon films obtained through electrochemical reduction of SiO_2 nanoparticles. *Thin Solid Films*, Vol. 654, 2018, pp. 1–10.

[237] Wenz, D. A., I. Johnson, and R. D. Wolson. $CaCl_2$-rich region of the $CaCl_2$-CaF_2-CaO system. *Journal of Chemical & Engineering Data*, Vol. 14, No. 2, 1969, pp. 250–252.

[238] Eastman, E. D., D. D. Cubicciotti, and C. D. Thurmond. Temperature-composition diagrams of metal-metal halide systems. *National Nuclear Energy Series Manhattan Project*, Vol. 19B, 1950, pp. 6–12.

[239] Suzuki, R. O., M. Aizawa, and K. O. Calcium-deoxidation of niobium and titanium in Ca-saturated $CaCl_2$ molten salt. *Journal of Alloys and Compounds*, Vol. 288, No. 1–2, 1999, pp. 173–182.

[240] Tago, Y., Y. Endo, K. Morita, F. Tsukihashi, and N. Sa. The activity of CaO in the CaO-$CaCl_2$ and CaO-$CaCl_2$-CaF_2 systems. *ISIJ International*, Vol. 35, No. 2, 1995, pp. 127–131.

[241] Ferro, P. D., B. Mishra, D. L. Olson, and W. A. Averill. Application of ceramic membrane in molten salt electrolysis of CaO-$CaCl_2$. *Waste Manage* (*Oxford*), Vol. 17, No. 7, 1998, pp. 451–461.

[242] Gao, P., X. Jin, D. Wang, X. Hu, and G. Z. Chen. A quartz sealed Ag/AgCl reference electrode for $CaCl_2$ based molten salts. *Journal of Electroanalytical Chemistry*, Vol. 579, No. 2, 2005, pp. 321–328.
[243] Schwandt, C. and D. J. Fray. The electrochemical reduction of chromium sesquioxide in molten calcium chloride under cathodic potential control. *Zeitschrift fur Naturforschung – Section A Journal of Physical Sciences*, Vol. 62, No. 10–11, 2007, pp. 655–670.
[244] Xiao, W., X. Jin, Y. Deng, D. Wang, and G. Z. Chen. Three-phase interlines electrochemically driven into insulator compounds: a penetration model and its verification by electroreduction of solid AgCl. *Chemistry – A European Journal*, Vol. 13, No. 2, 2007, pp. 604–612.
[245] Ma, Y., T. Yamamoto, K. Yasuda, and T. Nohira. Raman analysis and electrochemical reduction of silicate ions in molten NaCl–$CaCl_2$. *Journal of the Electrochemical Society*, Vol. 168, No. 4, 2021, id. 046515.
[246] Zhang, Q., Y. Hua, and R. Wang. Anodic oxidation of chloride ions in 1-butyl-3-methyl-limidazolium tetrafluoroborate ionic liquid. *Electrochimica Acta*, Vol. 105, 2013, pp. 419–423.
[247] Winand, R. Contribution to the study of electrocrystallization in fused salts. Application to the particular case of zirconium. *Mem Sci Rev Met*, Vol. 58, 1961, pp. 25–35.
[248] Winand, R. Electrocrystallization – theory and applications. *Hydrometallurgy*, Vol. 29, No. 1, 1992, pp. 567–598.
[249] Winand, R. Electrodeposition of metals and alloys—new results and perspectives. *Electrochimica Acta*, Vol. 39, No. 8, 1994, pp. 1091–1105.
[250] Fischer, H. *Elektrolytische Abscheidung und Elektrokristallisation von Metallen*, Springer Verlag, Berlin, 1954.
[251] Voltmer, F. V. and F. A. Padovani. The carbon silicon phase diagram for dilute carbon concentration and the influence of carbon on czochralski growth of silicon. *Semiconductor silicon*, Huff, H. R.and Burgess, R. R., (Eds.), The Electrochemical Society, Inc, Princeton, 1973, pp. 75–82.
[252] Banerjee, H. D., S. Sen, and H. N. Acharya. Investigations on the production of silicon from rice husks by the magnesium method. *Materials Science and Engineering*, Vol. 52, No. 2, 1982, pp. 173–179.
[253] Bose, D. N., P. A. Govindacharyulu, and H. D. Banerjee. Large grain polycrystalline silicon from rice husk. *Solar Energy Materials*, Vol. 7, No. 3, 1982, pp. 319–321.
[254] Mishra, P., A. Chakraverty, and H. D. Banerjee. Production and purification of silicon by calcium reduction of rice-husk white ash. *Journal of Materials Science*, Vol. 20, No. 12, 1985, pp. 4387–4391.
[255] Bessho, M., K. Umehara, T. Takaura, T. Nishiyama, and H. Shingu. The potential of production of high-purity silica from biogenic diatomaceous earth. *Shigen-to-Sozai*, Vol. 117, No. 9, 2001, pp. 736–742.
[256] Bessho, M., Y. Fukunaka, H. Kusuda, and T. Nishiyama. High-grade silica refined from diatomaceous earth for solar-grade silicon production. *Energy & Fuels*, Vol. 23, No. 8, 2009, pp. 4160–4165.
[257] Matsuo, N., Y. Matsui, Y. Fukunaka, and T. Homma. Solvent extraction using microchannel system for high purification of silica. *ECS Transactions*, Vol. 50, No. 48, 2013, pp. 103–108.
[258] Matsuo, N., Y. Matsui, Y. Fukunaka, and T. Homma. Boron extraction with 2-ethyl-1,3-hexanediol using a microchannel device for high-purity source of solar-grade silicon. *Journal of the Electrochemical Society*, Vol. 161, No. 5, 2014, pp. E93–E96.
[259] Homma, T., N. Matsuo, X. Yang, K. Yasuda, Y. Fukunaka, and T. Nohira. High purity silicon materials prepared through wet-chemical and electrochemical approaches. *Electrochimica Acta*, Vol. 179, 2015, pp. 512–518.
[260] Maeda, M. and A. McLean. Dissolution of carbon dioxide in calcium oxide-calcium chloride melts. *Iron Steelmaker*, Vol. 13, No. 9, 1986, pp. 61–65.
[261] Freidina, E. B. and D. J. Fray. Phase diagram of the system $CaCl_2$-$CaCO_3$. *Thermochimica Acta*, Vol. 351, No. 1–2, 2000, pp. 107–108.
[262] Mohamedi, M., B. Borresen, G. M. Haarberg, and R. Tunold. Anodic behavior of carbon electrodes in CaO-$CaCl_2$ melts at 1,123 K. *Journal of the Electrochemical Society*, Vol. 146, No. 4, 1999, pp. 1472–1477.
[263] Lebedev, V. A., V. I. Sal'nikov, M. V. Tarabaev, I. A. Sizikov, and D. A. Rymkevich. Kinetics and mechanism of the processes occurring at graphite anode in a CaO-$CaCl_2$ melt. *Russian Journal of Applied Chemistry*, Vol. 80, No. 9, 2007, pp. 1498–1502.
[264] Tunold, R., G. M. Haarberg, K. S. Osen, A. M. Martinez, and E. Sandnes. Anode processes on carbon in chloride-oxide melts. *ECS Transactions*, Vol. 35, No. 23, 2011, pp. 1–9.
[265] Trumbore, F. A. Solid solubilities of impurity elements in germanium and silicon. *Bell System Technical Journal*, Vol. 39, No. 1, 1960, pp. 205–233.
[266] Obinata, I. and N. Komatsu. Method of refining silicon by alloying – fundamental research. *Nippon Kinzoku Gakkai-shi* (*Journal of the Japan Institute of Metals and Materials*), Vol. 18, 1954, pp. 279–283.
[267] Obinata, I. and N. Komatsu. Method of refining silicon by alloying – experimentals in semi-industrial scale. *Nippon Kinzoku Gakkai-shi* (*Journal of the Japan Institute of Metals and Materials*), Vol. 18, 1954, pp. 283–285.
[268] Yoshikawa, T. and K. Morita. Removal of phosphorus by the solidification refining with Si-Al melts. *Science and Technology of Advanced Materials*, Vol. 4, No. 6, 2003, pp. 531–537.
[269] Yoshikawa, T. and K. Morita. Evaluation of segregation of B between solid Si and Si-Al melt. *CAMP-ISIJ*, Vol. 17, No. 4, 2004, id. 875.
[270] Yoshikawa, T. and K. Morita. Refining of silicon during its solidification from a Si–Al melt. *Journal of Crystal Growth*, Vol. 311, No. 3, 2009, pp. 776–779.
[271] Yoshikawa, T. and K. Morita. An evolving method for solar-grade silicon production: Solvent refining. *JOM*, Vol. 64, No. 8, 2012, pp. 946–951.
[272] Juneja, J. M. and T. K. Mukherjee. A study of the purification of metallurgical grade silicon. *Hydrometallurgy*, Vol. 16, No. 1, 1986, pp. 69–75.
[273] Mitrašinović, A. M. and T. A. Utigard. Refining silicon for solar cell application by copper alloying. *Silicon*, Vol. 1, No. 4, 2009, pp. 239–248.
[274] Ma, X., T. Yoshikawa, and K. Morita. Phase relations and thermodynamic property of boron in the silicon-tin melt at 1,673 K. *Journal of Alloys and Compounds*, Vol. 529, 2012, pp. 12–16.
[275] Hu, L., Z. Wang, X. Gong, Z. Guo, and H. Zhang. Impurities removal from metallurgical-grade silicon by combined Sn-Si and Al-Si refining processes. *Metallurgical and Materials Transactions B*, Vol. 44, No. 4, 2013, pp. 828–836.

[276] Ma, X., T. Yoshikawa, and K. Morita. Purification of metallurgical grade Si combining Si–Sn solvent refining with slag treatment. *Separation and Purification Technology*, Vol. 125, 2014, pp. 264–268.
[277] Esfahani, S. and M. Barati. Purification of metallurgical silicon using iron as an impurity getter part I: Growth and separation of Si. *Metals and Materials International*, Vol. 17, No. 5, 2011, pp. 823–829.
[278] Esfahani, S. and M. Barati. Purification of metallurgical silicon using iron as impurity getter, part II: Extent of silicon purification. *Metals and Materials International*, Vol. 17, No. 6, 2011, pp. 1009–1015.
[279] Khajavi, L. T., K. Morita, T. Yoshikawa, and M. Barati. Removal of boron from silicon by solvent refining using ferrosilicon alloys. *Metallurgical and Materials Transactions B*, Vol. 46, No. 2, 2015, pp. 615–620.
[280] Yin, Z., A. Oliazadeh, S. Esfahani, M. Johnston, and M. Barati. Solvent refining of silicon using nickel as impurity getter. *Canadian Metallurgical Quarterly*, Vol. 50, No. 2, 2011, pp. 166–172.
[281] Morito, H., T. Karahashi, M. Uchikoshi, M. Isshiki, and H. Yamane. Low-temperature purification of silicon by dissolution and solution growth in sodium solvent. *Silicon*, Vol. 4, No. 2, 2012, pp. 121–125.
[282] Ma, Y., K. Yasuda, A. Ido, T. Shimao, M. Zhong, R. Hagiwara, et al. Silicon refining by solidification from liquid Si–Zn Alloy and floating zone method. *Materials Transactions*, Vol. 62, No. 3, 2021, pp. 403–411.